

UCRHEP-T201 (August 1997)

CP Violation In Single Top Production And Decay Via $p\bar{p} \rightarrow t\bar{b} + X \rightarrow W^+b\bar{b} + X$ Within The MSSM: A Possible Application For Measuring $\arg(A_t)$ At Hadron Colliders

S. Bar-Shalom

Department of Physics, University of California at Riverside, Riverside CA 92521

D. Atwood

Theory Group, Thomas Jefferson National Accelerator Facility, Newport News, VA 23606
and

Department of Physics and Astronomy, Iowa State University, Ames, IA 50011¹

A. Soni

Physics Department, Brookhaven Nat. Lab., Upton NY 11973, USA.

Abstract

CP-nonconserving effects in the reaction $p\bar{p} \rightarrow t\bar{b} + X \rightarrow W^+b\bar{b} + X$, driven by the supersymmetric CP-odd phase of the stop trilinear soft breaking term, $\arg(A_t)$, are studied. We discuss the CP-nonconserving effects in both production and the associated decay amplitudes of the top. We find that, within a plausible low energy scenario of the MSSM and keeping the neutron electric dipole moment below its current limit, a CP-violating cross-section asymmetry as large as 2 – 3% can arise if some of the parameters lie in a favorable range. A partial rate asymmetry originating only in the top decay $t \rightarrow W^+b$ is found to be, in general, below the 0.1% level which is somewhat smaller than previous claims. For a low $\tan\beta$ of order one the decay asymmetry can reach at the most $\sim 0.3\%$. This (few) percent level overall CP-violating signal in $p\bar{p} \rightarrow t\bar{b} + X \rightarrow W^+b\bar{b} + X$ might be within the reach of the future 2(4) TeV $p\bar{p}$ Tevatron collider that may be able to produce $\sim 10000(\sim 30000)$ such $t\bar{b}$ events with an integrated luminosity of 30 fb^{-1} . In particular, it may be used to place an upper bound on $\arg(A_t)$ if indeed $\arg(\mu) \rightarrow 0$, as implied from the present experimental limit on the neutron electric dipole moment. The partial rate asymmetry in the top decay ($\sim \text{few} \times 10^{-3}$) may also be within the reach of the LHC with $\sim 10^7$ pairs of $t\bar{t}$ produced, provided detector systematics are sufficiently small. We also show that if the GUT-scale universality of the soft breaking trilinear A terms is relaxed, then the phases associated with $\arg A_u$ and $\arg A_d$ can take values up to $\sim \text{few} \times 10^{-1}$ even with squarks and gluino masses of several hundred GeV's without contradicting the experimental limit on the neutron electric dipole moment.

¹Address after August 1, 1997.

1. Introduction

In the Tevatron $p\bar{p}$ collider, top quarks will be mainly produced as pairs of $t\bar{t}$ via an s -channel gluon exchange. Nonetheless, the subleading ElectroWeak (EW) production mechanism of a single top, forms a significant fraction of the $t\bar{t}$ pair production. It will therefore be closely scrutinized in the next runs of the Tevatron [1]. In particular, the production rate of $t\bar{b}$ (and the charged conjugate pair) through an s -channel W -boson, $p\bar{p} \rightarrow W \rightarrow t\bar{b} + X$, (the corresponding partonic reaction is $u\bar{d} \rightarrow W \rightarrow t\bar{b}$) is about 10% of the $t\bar{t}$ production rate [1]. Throughout this paper we will always refer only to the s -channel W exchange when discussing the reaction $p\bar{p} \rightarrow t\bar{b} + X$.

In a previous work, [2], we have shown that a new CP-violating phase from a Two Higgs Doublet Model (2HDM) of type II can give rise to CP-violating asymmetries of the order of a few percent in the reaction $p\bar{p} \rightarrow t\bar{b} + X$. In that work we had considered one example of a supersymmetric (SUSY) mediated, one-loop, CP-violating diagram (gluino exchange diagram). The one SUSY diagram that was considered in [2] was found to be p-wave suppressed near threshold, thus yielding CP asymmetries of the order of 0.1%. Clearly a complete study of the possible SUSY-CP effect is required in order to be able to estimate the true expected magnitude of a potential CP-nonconserving effect that is driven by new CP-odd phases of low energy SUSY dynamics.

Therefore, in this paper we wish to extend our previous study and explore the complete CP-violating effect in the process $p\bar{p} \rightarrow t\bar{b} + X \rightarrow W^+b\bar{b} + X$, induced specifically by the complex soft trilinear parameter associated with the superpartner of the top, A_t , in the Minimal Supersymmetric Standard Model (MSSM). We will separately discuss the SUSY CP-nonconserving effect in production and decay amplitudes of the top and show how these two asymmetries combine to give the overall asymmetry in $p\bar{p} \rightarrow t\bar{b} + X \rightarrow W^+b\bar{b} + X$.

The experimental limit on the Neutron Electric Dipole Moment (NEDM), $d_n \leq 1.1 \times 10^{-25}$ e-cm [3], places a severe constraint on the phase of the SUSY Higgs mass parameter μ . In particular, $\arg(\mu) < \mathcal{O}(10^{-2})$ [4, 5, 6, 7] is essentially inevitable for a typical SUSY mass scale of the order of a few hundreds GeV. Therefore, the *only significant* SUSY-CP-odd phase, that can potentially drive notable CP-nonconserving effects in top quark reactions, is the phase in the stop soft trilinear breaking term A_t . As will be shown below, CP-violating effects that can arise from the other A_{q_i} terms (associated with the lighter quarks q_i) are extremely suppressed being proportional to the masses of the light quarks. In particular, when $m_{q_i} \rightarrow 0$ there is no mixing between the left and the right squarks. The two mass eigenstates of the supersymmetric partners of the light quarks are therefore expected to be nearly degenerate, thus not playing any role in CP-violation effects at high

enough energies. Of course, this is not the case for the NEDM which is driven by the slight deviation from degeneracy of the supersymmetric partners of the u and the d quarks when $\arg(\mu) = 0$.

Moreover, if the phases of A_u, A_d and A_t are not correlated at the EW scale, which is indeed possible if the GUT-scale universality of the A terms is relaxed, then the experimental limit on the NEDM cannot put any further constraint on $\arg(A_t)$. Therefore, it is extremely important to explore other avenues for constraining $\arg(A_t)$. Of course, the most natural place to look for CP-nonconserving effects, which are driven by $\arg(A_t)$, is high energy reactions involving the top quark. Thus, in the limit $\arg(\mu) \rightarrow 0$, the *only* important phenomenological CP-violating SUSY parameter, that enters any CP-odd effect at high energies, resides in the imaginary part of the $\tilde{t}_L - \tilde{t}_R$ mixing matrix elements $\text{Im}(Z_t^{1i*} Z_t^{2i})$ (see appendix A). Being proportional to $\arg(A_t)$, it vanishes for $\arg(A_t) \rightarrow 0$. Besides, $\arg(A_t)$ may play an important role in explaining the observed baryon asymmetry in the universe. Recently, it was claimed that with $\arg(\mu) \rightarrow 0$, t squarks can mediate the charge transport mechanism needed to generate the observed baryon asymmetry even with squark masses $\sim \text{few} \times \text{GeV}$, provided that $\arg(A_t)$ is not much suppressed [8].

In this paper we discuss the CP-odd effects, induced by $\text{Im}(Z_t^{1i*} Z_t^{2i}) \propto \arg(A_t)$ in the reaction $p\bar{p} \rightarrow t\bar{b} + X$ and in the subsequent top decay $t \rightarrow W^+b$. We find that, with maximum CP-violation (i.e., $|\text{Im}(Z_t^{1i*} Z_t^{2i})| = 1/2$), a CP-violating asymmetry in the cross-section can reach 3% for squark masses at around 0.5 TeV and a light stop mass below 100 GeV. We also find that, in the same range of squark masses, a Partial Rate Asymmetry (PRA) effect in $t \rightarrow W^+b$ is predominantly below 0.1% and can be slightly above 0.1% for low $\tan\beta$. In a narrow window of the SUSY parameter space, with $\tan\beta \sim \mathcal{O}(1)$, it can reach at the most $\sim 0.3\%$. This is somewhat less than the estimates in the literature of a few percent asymmetry in top decay in the MSSM [9]. Therefore, with a predicted few percent overall asymmetry in the cross-section and decay, the reaction $p\bar{p} \rightarrow t\bar{b} + X \rightarrow W^+b\bar{b} + X$ can serve to constrain $\arg(A_t)$ in the future runs of the upgraded Tevatron at Fermilab.

Also, as a by product of our analysis, we found that when the Higgs mass term, μ , is real at the EW-scale (or has a very small phase) and bearing theoretical uncertainties associated with the naive quark model approach (see e.g., [10]), the experimental limit on the NEDM can be naturally accommodated with phases of the soft trilinear breaking A terms at the order of $\sim \text{few} \times 10^{-1}$ even with squark and gluino masses below 500 GeV. Therefore, we believe that there is no compelling argument for the SUSY CP-odd phases to be necessarily less than or of the order of 10^{-2} for squarks masses below 1 TeV, contrary to previously and commonly used claims.

We wish to emphasize that the analytical formulations given in this paper hold for the most general low energy realization of the MSSM. Moreover, the PRA effect in the top decay $t \rightarrow W^+b$,

presented in this paper, does not depend on the specific production mechanism of the t and \bar{t} . Therefore, the LHC which may be able to produce $\sim 10^7$ pairs of $t\bar{t}$ may, in principle, be able to detect a PRA effect in $t \rightarrow W^+b$ even as small as $\sim \text{few} \times 10^{-3}$, provided detector systematics are sufficiently small.

The paper is organized as follows: in section 2 we construct a plausible phenomenological low energy SUSY spectrum. In section 3 we present a complete, self contained analytical derivation of the CP asymmetry in both production and decay processes of the top in a general MSSM framework, keeping all possible SUSY CP-odd phases. In section 4 we discuss our choice of the low energy CP phases and its implications on the NEDM. In section 5 we present our numerical results in the limit $\arg(\mu) = 0$ and in section 6 we summarize. The relevant SUSY lagrangian pieces along with a detailed derivation of the various SUSY mixing matrix elements is given in appendix A. In appendix B we list the SUSY CP-violating phases, in the general MSSM scenario, that are responsible for the CP-asymmetry in our reaction while a description of the one-loop integrals is given in appendix C.

2. Low Energy MSSM Phenomenology

The most general low energy $N = 1$ minimal supergravity (SUGRA) $SU(3) \times SU(2) \times U(1)$ invariant lagrangian (which apart from gravitational interactions, is essentially identical at low energies to a theory with softly broken supersymmetry), that consists of three generations of quarks, two Higgs doublets and the $SU(3) \times SU(2) \times U(1)$ gauge fields, along with their supersymmetric partners, can be written as [11, 12, 13]:

$$\mathcal{L} = \text{kinetic terms} + \int d^2\theta W + \mathcal{L}_{\text{soft}} \quad , \quad (1)$$

where W is the superpotential and is given by:

$$W = \epsilon_{ij}(g_U^{IJ} \hat{Q}_I^i \hat{H}_2^j \hat{U}_J + g_D^{IJ} \hat{Q}_I^i \hat{H}_1^j \hat{D}_J^c + g_E^{IJ} \hat{L}_I^i \hat{H}_1^j \hat{R}_J^c + \mu \hat{H}_1^i \hat{H}_2^j) \quad . \quad (2)$$

ϵ_{ij} is the antisymmetric tensor with $\epsilon_{12} = 1$ and the usual convention was used for the superfields $\hat{Q}, \hat{U}, \hat{L}, \hat{R}$ and \hat{H} [11]. The capital index indicates the generation (i.e., $I, J = 1, 2$ or 3).

$\mathcal{L}_{\text{soft}}$ consists of the soft breaking terms and can be divided into three pieces:

$$\mathcal{L}_{\text{soft}} \equiv \mathcal{L}_{\text{gaugino}} + \mathcal{L}_{\text{scalar}} + \mathcal{L}_{\text{trilinear}} \quad . \quad (3)$$

These are the soft-supersymmetry breaking gaugino and scalar mass terms and the trilinear coupling breaking terms. In particular they are given by [13]:

$$\mathcal{L}_{\text{gaugino}} = \frac{1}{2}(\tilde{m}_1\lambda_B\lambda_B + \tilde{m}_2\lambda_W^a\lambda_W^a + \tilde{m}_3\lambda_G^b\lambda_G^b) \quad , \quad (4)$$

$$\begin{aligned} \mathcal{L}_{\text{scalar}} = & -m_{H_1}^2|H_i^1|^2 - m_{H_2}^2|H_i^2|^2 - m_L^2|L^i|^2 - \\ & m_R^2|R|^2 - m_Q^2|Q^i|^2 - m_D^2|D|^2 - m_U^2|U|^2 \quad , \end{aligned} \quad (5)$$

$$\begin{aligned} \mathcal{L}_{\text{trilinear}} = & \epsilon_{ij}(g_U A_U Q^i H_2^j U + g_D A_D Q^i H_1^j D + \\ & g_E A_E L^i H_1^j R + \mu B H_1^i H_2^j) \quad . \end{aligned} \quad (6)$$

In the above soft breaking terms we have omitted the family indices I and J . The above scalar fields correspond to the superfields which were indicated in our notation by a “hat”. λ_B , λ_W^a (with $a = 1, 2$ or 3) and λ_G^b (with $b = 1, \dots, 8$) are the gauge superpartners of the U(1), SU(2) and SU(3) gauge bosons, respectively.

The conventional wisdom is to assume a complete universality of the soft supersymmetric parameters at the GUT scale. That is, a common scalar mass m_0 , a common gaugino mass $M_{1/2}$ and a universal boundary condition for the trilinear soft breaking terms $A_U = A_D = A_E = A^G$. This gives rise to an appealing theory with a minimum number of free parameters, which, among other interesting features, allows Radiative EW Symmetry Breaking (REWSB) [14]. Such a SUGRA model has only two independent CP-violating phases at the GUT scale [15]. These two physical phases can be chosen as $\arg(A^G)$ and $\arg(\mu^G)$. Nonetheless, although very attractive, a complete universality of the soft breaking terms at the GUT scale (motivated by a “would be” GUT-scale SUGRA model scenario) is a simplifying assumption. If the universality of the trilinear soft breaking terms mentioned above is relaxed, REWSB can still occur. Yet, in this less constrained framework, the A_t , A_u and A_d (the only three soft trilinear breaking terms relevant for our discussion in this paper) can have different phases at the GUT scale, and therefore their phases at the EW scale are completely undetermined. As a consequence, we will show below that, contrary to previous claims, with no “fine tuning” of $\arg(A_u)$ and $\arg(A_d)$, the NEDM can meet its experimental limit even with squark masses of a few hundred GeV, leaving $\arg(A_t)$ large enough to drive significant CP-violating effects in top quark systems. We will discuss in detail the “SUSY CP problem” of the NEDM in section 4.

Till now, no supersymmetric particle has been discovered, and in spite of the very fascinating theoretical features of the GUT-scale SUGRA model, there is no experimental hint that can indicate

the real nature of the underlying, short distance SUSY model. We therefore wish to keep an open mind and instead of restricting ourselves to the GUT-scale SUGRA model with complete universality of the soft breaking terms, our strategy will be to choose a plausible set of the SUSY parameters at the EW scale subject to the present experimental limits on the sparticle masses [16]. Indeed, by relaxing the GUT-scale universality of only the soft breaking trilinear A terms, almost any low energy SUSY spectrum can be consistently recovered.

We now describe the key features and assumptions of our low energy SUSY scenario:

I) Motivated by the strong theoretical prediction of the unification of the SU(3), SU(2) and U(1) gauge couplings when SUSY particles with a mass scale around 1 TeV are folded into the Renormalization Group Equations (RGE), we will follow only one traditional simplifying GUT assumption; that there is an underlying grand unification. This leads us to have a common gaugino mass parameter defined at the GUT scale. Then, the difference between the three low energy gaugino mass parameters comes from the fact that they undergo a different renormalization when they evolve from the GUT scale to the EW scale due to the different gauge structure of their interactions. The gaugino masses, at the EW-scale, are then related by [17]:

$$\frac{3 \cos^2 \theta_W}{5} \frac{\tilde{m}_1}{\alpha} = \sin^2 \theta_W \frac{\tilde{m}_2}{\alpha} = \frac{\tilde{m}_3}{\alpha_s}, \quad (7)$$

where θ_W is the weak mixing angle and \tilde{m}_3 is the low energy gluino mass (from now on, we will refer to the gluino mass as m_G). Thus, once the gluino mass is set at the EW scale, the SU(2) and U(1) gaugino masses \tilde{m}_2 and \tilde{m}_1 , respectively, are determined.

II) All the squarks except for the light stop are assumed to be degenerate with a mass M_s , while the light stop mass, which we denote by m_t , is chosen subject to $m_t > 50$ GeV [16].

III) The mass matrices of the neutralinos, $M_{\tilde{\chi}^0}$, and charginos, $M_{\tilde{\chi}}$, depend on the low energy Higgs mass parameter μ , the two gaugino masses \tilde{m}_2 and \tilde{m}_1 (which are resolved by the gluino mass) and $\tan \beta$ (see appendix A). Therefore, once μ , m_G and $\tan \beta$ are set to their low energy values, the four physical neutralino species $m_{\tilde{\chi}_n^0}$ ($n = 1 - 4$) and the two physical chargino species $m_{\tilde{\chi}_m}$ ($m = 1, 2$) are extracted by diagonalizing $M_{\tilde{\chi}^0}$ and $M_{\tilde{\chi}}$. In appendix A we list the full analytical prescription for diagonalizing the neutralinos and charginos mixing matrices in the case that μ is real.

IV) We limit the lightest neutralino mass to be above 20 GeV and the lighter chargino mass to be above 65 GeV [16].

V) We will always choose $m_G > 200$ GeV within the range $M_s - 200$ GeV $\lesssim m_G \lesssim M_s + 200$ GeV as roughly indicated by recent results from the Tevatron [16].

With no further assumptions, the low energy SUSY mass spectrum is fully determined from the only five free parameters μ, m_G, M_s, m_t and $\tan\beta$. The possible CP phases, that can arise in this low energy SUSY framework, will be described in detail in section 4.

3. Derivation of the CP Violating Asymmetry

We now turn to the discussion of the possible CP-violating effects in the process $p\bar{p} \rightarrow t\bar{b} + X \rightarrow W^+b\bar{b} + X$ (i.e., production of a pair of $t\bar{b}$ followed by the top decay $t \rightarrow bW^+$), driven by SUSY CP-violating sources [18]. To estimate the possible size of the effect, we consider the following CP-violating quantity:

$$\hat{A} \equiv \frac{\hat{\sigma}(\hat{s}) - \hat{\bar{\sigma}}(\hat{s})}{\hat{\sigma}(\hat{s}) + \hat{\bar{\sigma}}(\hat{s})}, \quad (8)$$

where $\hat{s} = (p_t + p_b)^2$ and $\hat{\sigma}(\hat{s})$ and $\hat{\bar{\sigma}}(\hat{s})$ are the cross-sections for the reactions $u\bar{d} \rightarrow t\bar{b} \rightarrow W^+b\bar{b}$ and $\bar{u}d \rightarrow \bar{t}b \rightarrow W^-\bar{b}b$, respectively. Folding in the parton densities in the usual manner [19] we define the asymmetry of cross-sections at the level of the colliding protons as:

$$A \equiv \frac{\sigma(s) - \bar{\sigma}(s)}{\sigma(s) + \bar{\sigma}(s)}. \quad (9)$$

Now $s = (p_p + p_{\bar{p}})^2$ and $\sigma(s)$ and $\bar{\sigma}(s)$ are the cross sections for $p\bar{p} \rightarrow t\bar{b} + X \rightarrow W^+b\bar{b} + X$ and $p\bar{p} \rightarrow \bar{t}b + X \rightarrow W^-\bar{b}b + X$, respectively.

In the narrow width approximation the tree-level cross-section at the quark level is given by:

$$\hat{\sigma}_0(\hat{s}) \approx \frac{\pi\alpha^2(m_t^2 - \hat{s})^2(m_t^2 + 2\hat{s})}{24\sin^4\theta_W\hat{s}^2(\hat{s} - m_W^2)^2} \times \text{Br}(t \rightarrow W^+b). \quad (10)$$

In Fig. 1 we have drawn the tree level diagram for the parton level reaction $u\bar{d} \rightarrow t\bar{b}$. The possible supersymmetric one loop diagrams that can violate CP invariance in this reaction are depicted in Fig. 2. Note that in both Fig. 1 and 2 the subsequent top decay is not explicitly drawn. The one-loop CP-violating triangle diagrams a-d of Fig. 2 in the production vertex will enter also the top decay $t \rightarrow W^+b$ with the t and W^+ momenta reversed.

To one-loop order in perturbation theory, where the CP-violating virtual corrections enter only either the production or the decay vertices of the top in the overall reaction $p\bar{p} \rightarrow t\bar{b} + X \rightarrow W^+b\bar{b} + X$, and in the narrow width approximation for the decaying top, the overall CP asymmetry, A , can be broken into:

$$A = A_P + A_D . \quad (11)$$

In this Eq. A_P and A_D are the CP asymmetries emanating from the production and decay of the top, respectively, and are defined by:

$$A_P \equiv \frac{\sigma(p\bar{p} \rightarrow t\bar{b} + X) - \bar{\sigma}(p\bar{p} \rightarrow \bar{t}b + X)}{\sigma(p\bar{p} \rightarrow t\bar{b} + X) + \bar{\sigma}(p\bar{p} \rightarrow \bar{t}b + X)} , \quad (12)$$

$$A_D \equiv \frac{\Gamma(t \rightarrow W^+b) - \bar{\Gamma}(\bar{t} \rightarrow W^-\bar{b})}{\Gamma(t \rightarrow W^+b) + \bar{\Gamma}(\bar{t} \rightarrow W^-\bar{b})} . \quad (13)$$

The PRA A_D , defined in Eq. 13, is an independent quantity and does not depend on the specific production mechanism of the top. We will therefore treat the CP-nonconserving asymmetries A_P and A_D separately keeping in mind that the total CP-odd effect is simply the sum of the two. Moreover, it is convenient to further divide the cross-section asymmetry in $t\bar{b}$ production, A_P , into:

$$A_P \equiv A_P^{\text{triangle}} + A_P^{\text{box}} , \quad (14)$$

where A_P^{triangle} and A_P^{box} are the CP-violating cross-section asymmetries which arise from the triangle diagrams $a-d$ and $a'-d'$ and box diagrams $e-h$ in Fig. 2, respectively. Similarly, the corresponding parton level asymmetries will be denoted by a ‘‘hat’’.

Asymmetry From Triangle Diagrams In The Production Amplitude - A_P^{triangle} :

The one-loop $t\bar{b}$ and $\bar{t}b$ currents of the production amplitude can be parameterized as:

$$J_k^{\mu(t\bar{b})} \equiv i \frac{g_W}{\sqrt{2}} \sum_{P=L,R} \bar{u}_t \left(\frac{\mathcal{P}_{1(k)}^P p_b^\mu}{m_t} + \mathcal{P}_{2(k)}^P \gamma^\mu \right) P v_b , \quad (15)$$

$$J_k^{\mu(\bar{t}b)} \equiv i \frac{g_W}{\sqrt{2}} \sum_{P=L,R} \bar{u}_b \left(\frac{\bar{\mathcal{P}}_{1(k)}^P p_b^\mu}{m_t} + \bar{\mathcal{P}}_{2(k)}^P \gamma^\mu \right) P v_t , \quad (16)$$

where $P = L$ or R and $L(R) \equiv (1 - (+)\gamma_5)/2$. The index k indicates the triangle diagram (i.e. $k = a, b, c, d, a', b', c'$ or d'). $\mathcal{P}_{1(k)}^{L,R}$ and $\mathcal{P}_{2(k)}^{L,R}$ defined in Eqs. 15 and 16, contain the SUSY CP-violating phases as well as the absorptive phases of the triangle diagrams, both of which are needed to render A_P^{triangle} non-zero. Then, in terms of the scalar ($\mathcal{P}_{1(k)}$) and vector ($\mathcal{P}_{2(k)}$) form factors, the parton level cross-section asymmetry $\hat{A}_P^{\text{triangle}}$ is given by:

$$\hat{A}_P^{\text{triangle}} = \sum_k \left\{ \frac{(x-1)}{2(x+2)} \text{Re}(\mathcal{P}_{1(k)}^L + \bar{\mathcal{P}}_{1(k)}^R) - \text{Re}(\mathcal{P}_{2(k)}^L - \bar{\mathcal{P}}_{2(k)}^L) \right\}, \quad (17)$$

where $x \equiv m_t^2/\hat{s}$ and the sum is carried out over all triangle diagrams in Fig. 2. It is easy to show that if one defines:

$$\mathcal{P}_{1(k)}^L \sim e^{i\delta_s^{1(k)}} \times e^{i\delta_w^{1(k)}}, \quad (18)$$

$$\mathcal{P}_{2(k)}^L \sim e^{i\delta_s^{2(k)}} \times e^{i\delta_w^{2(k)}}, \quad (19)$$

where $\delta_s^{1(k)}, \delta_s^{2(k)}$ are the CP-even absorptive phases (i.e., final state interaction phases) and $\delta_w^{1(k)}, \delta_w^{2(k)}$ are the CP-odd phases associated with each of the triangle diagrams in Fig. 2, then:

$$\bar{\mathcal{P}}_{1(k)}^R \sim -e^{i\delta_s^{1(k)}} \times e^{-i\delta_w^{1(k)}}, \quad (20)$$

$$\bar{\mathcal{P}}_{2(k)}^L \sim e^{i\delta_s^{2(k)}} \times e^{-i\delta_w^{2(k)}}. \quad (21)$$

The CP-violating scalar form factors in Eq. 17, for each triangle diagram are then given by:

$$\text{Re}(\mathcal{P}_{1(a)}^L + \bar{\mathcal{P}}_{1(a)}^R) = \frac{8}{3} \frac{\alpha_s}{\pi} m_t m_{\tilde{g}} \mathcal{O}_a^1 (C_0^a + C_{11}^a), \quad (22)$$

$$\text{Re}(\mathcal{P}_{1(b)}^L + \bar{\mathcal{P}}_{1(b)}^R) = -\frac{\alpha}{\pi \sin^2 \theta_W} m_t \left[m_t \mathcal{O}_b^1 (C_{12}^b + C_{23}^b) - m_{\tilde{\chi}_n^0} \mathcal{O}_b^2 (C_0^b + C_{11}^b) \right], \quad (23)$$

$$\begin{aligned} \text{Re}(\mathcal{P}_{1(c)}^L + \bar{\mathcal{P}}_{1(c)}^R) &= -\frac{\alpha}{\pi \sin^2 \theta_W} m_t \left[m_t \mathcal{O}_c^1 (C_{12}^c + C_{23}^c) + m_{\tilde{\chi}_m} \mathcal{O}_c^2 C_{12}^c \right. \\ &\quad \left. + m_{\tilde{\chi}_n^0} \mathcal{O}_c^3 (C_{12}^c - C_{11}^c) \right], \end{aligned} \quad (24)$$

$$\text{Re}(\mathcal{P}_{1(d)}^L + \bar{\mathcal{P}}_{1(d)}^R) = \text{Re}(\mathcal{P}_{1(c)}^L + \bar{\mathcal{P}}_{1(c)}^R) \left(m_{\tilde{\chi}_n^0} \rightarrow -m_{\tilde{\chi}_m}, m_{\tilde{\chi}_m} \rightarrow m_{\tilde{\chi}_n^0}, \mathcal{O}_c^i \rightarrow \mathcal{O}_d^i, C_{ij}^c \rightarrow C_{ij}^d \right), \quad (25)$$

and the CP-violating vector form factors in Eq. 17 are:

$$\text{Re}(\mathcal{P}_{2(a)}^L - \bar{\mathcal{P}}_{2(a)}^L) = 0, \quad (26)$$

$$\text{Re}(\mathcal{P}_{2(b)}^L - \bar{\mathcal{P}}_{2(b)}^L) = \frac{\alpha}{\pi \sin^2 \theta_W} \mathcal{O}_b^1 C_{24}^b, \quad (27)$$

$$\begin{aligned} \text{Re}(\mathcal{P}_{2(c)}^L - \bar{\mathcal{P}}_{2(c)}^L) &= \frac{1}{2} \frac{\alpha}{\pi \sin^2 \theta_W} \left[\mathcal{O}_c^1 \left((\hat{s} - m_t^2) C_{23}^c - \hat{s} C_{22}^c - 2C_{24}^c - m_t^2 C_{12}^c \right) \right. \\ &\quad \left. - m_t m_{\tilde{\chi}_m} \mathcal{O}_c^2 C_{12}^c - m_t m_{\tilde{\chi}_n^0} \mathcal{O}_c^3 (C_0^c + C_{12}^c) \right] \end{aligned}$$

$$-m_{\tilde{\chi}_m} m_{\tilde{\chi}_n^0} \mathcal{O}_c^4 C_0^c] , \quad (28)$$

$$\text{Re}(\mathcal{P}_{2(d)}^L - \bar{\mathcal{P}}_{2(d)}^L) = \text{Re}(\mathcal{P}_{2(c)}^L - \bar{\mathcal{P}}_{2(c)}^L) \left(m_{\tilde{\chi}_n^0} \rightarrow -m_{\tilde{\chi}_m}, m_{\tilde{\chi}_m} \rightarrow m_{\tilde{\chi}_n^0}, \mathcal{O}_c^i \rightarrow \mathcal{O}_d^i, C_{ij}^c \rightarrow C_{ij}^d \right) , \quad (29)$$

$$\text{Re}(\mathcal{P}_{2(a')}^L - \bar{\mathcal{P}}_{2(a')}^L) = 0 , \quad (30)$$

$$\text{Re}(\mathcal{P}_{2(b')}^L - \bar{\mathcal{P}}_{2(b')}^L) = -\frac{\alpha}{\pi \sin^2 \theta_W} \mathcal{O}_{b'}^1 C_{24}^{b'} , \quad (31)$$

$$\begin{aligned} \text{Re}(\mathcal{P}_{2(c')}^L - \bar{\mathcal{P}}_{2(c')}^L) &= \frac{1}{2} \frac{\alpha}{\pi \sin^2 \theta_W} \left[\mathcal{O}_{c'}^1 \left(\hat{s}(C_{23}^{c'} - C_{22}^{c'}) - 2C_{24}^{c'} \right) \right. \\ &\quad \left. + m_{\tilde{\chi}_m} m_{\tilde{\chi}_n^0} \mathcal{O}_{c'}^2 C_0^{c'} \right] , \end{aligned} \quad (32)$$

$$\text{Re}(\mathcal{P}_{2(d')}^L - \bar{\mathcal{P}}_{2(d')}^L) = \text{Re}(\mathcal{P}_{2(c')}^L - \bar{\mathcal{P}}_{2(c')}^L) \left(m_{\tilde{\chi}_n^0} \rightarrow -m_{\tilde{\chi}_m}, m_{\tilde{\chi}_m} \rightarrow m_{\tilde{\chi}_n^0}, \mathcal{O}_{c'}^i \rightarrow \mathcal{O}_{d'}^i, C_{ij}^{c'} \rightarrow C_{ij}^{d'} \right) \quad (33)$$

The SUSY CP-weak phases associated with the triangle diagrams, the \mathcal{O}_k^i 's above, are given in appendix B and all the corresponding loop form factors C_0^k, C_{pq}^k ($p = 1, 2$ and $q = 1 - 4$) are defined and given in appendix C.

Note that for diagrams a', b', c' and d' only a vector form factor in the $u\bar{d}$ one-loop current contributes to CP-violation in the limit $m_u, m_d \rightarrow 0$ (in this limit diagram a' contain no CP-violating phase). That is:

$$J_k^{\mu(u\bar{d})} \equiv i \frac{g_W}{\sqrt{2}} \sum_{P=L,R} \bar{v}_d \mathcal{P}_{2(k)}^P \gamma^\mu P u_u , \quad (34)$$

$$J_k^{\mu(\bar{u}d)} \equiv i \frac{g_W}{\sqrt{2}} \sum_{P=L,R} \bar{v}_u \bar{\mathcal{P}}_{2(k)}^P \gamma^\mu P u_d . \quad (35)$$

and we can therefore consider these diagrams to have the same structure as diagrams a, b, c and d (see Eqs. 15 and 16), taking the vector form factor in the ud current to be the vector form factor in the tb current.

Asymmetry From Box Diagrams In The Production Amplitude - A_P^{box} :

There are two kinds of amplitudes for the box diagrams. The amplitudes for diagrams e and f in Fig. 2 can be written schematically as:

$$-i\mathcal{M}_{k=e,f} \equiv \frac{-g_W^4}{16\pi^2} \int \frac{d^4 q}{i\pi^2} \left\{ \frac{\bar{u}_t \left[\sum_{P=L,R} \left(\mathcal{X}_k^P + \mathcal{X}_k'^P \not{p}_1 \right) P \right] u_u \bar{v}_d \left[\sum_{P=L,R} \left(\mathcal{Y}_k^P + \mathcal{Y}_k'^P \not{p}_2 \right) P \right] v_b}{\mathcal{A}_k^1 \mathcal{A}_k^2 \mathcal{A}_k^3 \mathcal{A}_k^4} \right\} , \quad (36)$$

whereas for Diagrams g and h :

$$-i\mathcal{M}_{k=g,h} \equiv \frac{-g_W^4}{16\pi^2} \int \frac{d^4q}{i\pi^2} \left\{ \frac{\bar{u}_t \left[\sum_{P=L,R} \left(\mathcal{X}_k^P + \mathcal{X}_k'^P \not{p}_1 \right) P \right] u_d \bar{u}_b \left[\sum_{P=L,R} \left(\mathcal{Y}_k^P + \mathcal{Y}_k'^P \not{p}_2 \right) P \right] u_u}{\mathcal{A}_k^1 \mathcal{A}_k^2 \mathcal{A}_k^3 \mathcal{A}_k^4} \right\}. \quad (37)$$

The four vectors p_1 and p_2 , that appear in Eqs. 36 and 37 above, stand for either q - the integrated four momentum in the loop or $p = p_t + p_b$ - the \hat{s} -channel four momentum. Also, the denominators \mathcal{A}_k^i of the particles in the loop can be read off appendix C (see also [20]).

A straight forward calculation of the interference of diagrams e, f, g and h with the tree level diagram yields:

$$\hat{A}_P^{\text{box}} = \frac{3}{2} \frac{\alpha}{\pi \sin^2 \theta_W} \frac{(y-1)}{(1-x)^2(2+x)} \sum_k \frac{1}{\hat{s}^2} \int_{\hat{t}^- = m_t^2 - \hat{s}}^{\hat{t}^+ = 0} d\hat{t} \left\{ \mathcal{B}_k^1(\hat{s}, \hat{t}) + \mathcal{B}_k^2(\hat{s}, \hat{t}) \right\}, \quad (38)$$

where $y \equiv m_W^2/\hat{s}$ and the three Mandelstam variables at the parton level (i.e., \hat{s}, \hat{t} and \hat{u}) are related via (for $m_b = m_u = m_d = 0$) $\hat{s} + \hat{t} + \hat{u} = m_t^2$. For later use, we furthermore define the following quantity:

$$X \equiv \frac{1}{2} \left[\hat{s} (\hat{s} - m_t^2) - \hat{t} (\hat{t} - m_t^2) + \hat{u} (\hat{u} - m_t^2) \right]. \quad (39)$$

For diagrams e and f , in the limit $m_u = m_d = m_b \rightarrow 0$, the $\mathcal{X}_k^R, \mathcal{X}_k'^R, \mathcal{Y}_k^L, \mathcal{Y}_k^R$ and $\mathcal{Y}_k'^R$ terms do not contribute to \hat{A}_P^{box} and we get:

$$\mathcal{B}_{k=e,f}^1(\hat{s}, \hat{t}) = 2m_t \text{Im} \left(\mathcal{X}_k^L \mathcal{Y}_k'^L \right) \text{Im} \left(\int \frac{d^4q}{i\pi^2} \left\{ \frac{\text{Tr} [L \not{p}_u \not{p}_b (\not{q} - \not{p}) \not{p}_d]}{\mathcal{A}_k^1 \mathcal{A}_k^2 \mathcal{A}_k^3 \mathcal{A}_k^4} \right\} \right), \quad (40)$$

$$\mathcal{B}_{k=e,f}^2(\hat{s}, \hat{t}) = 2 \text{Im} \left(\mathcal{X}_k'^L \mathcal{Y}_k^L \right) \text{Im} \left(\int \frac{d^4q}{i\pi^2} \left\{ \frac{\text{Tr} [L \not{p}_t \not{q} \not{p}_u \not{p}_b (\not{q} - \not{p}) \not{p}_d]}{\mathcal{A}_k^1 \mathcal{A}_k^2 \mathcal{A}_k^3 \mathcal{A}_k^4} \right\} \right), \quad (41)$$

whereas, for diagrams g and h the $\mathcal{X}_k^L, \mathcal{X}_k'^L, \mathcal{Y}_k^R, \mathcal{Y}_k'^L$ and $\mathcal{Y}_k'^R$ terms vanish, and we have:

$$\mathcal{B}_{k=g,h}^1(\hat{s}, \hat{t}) = -2\hat{u} \text{Im} \left(\mathcal{X}_k^R \mathcal{Y}_k^L \right) \text{Im} \left(\int \frac{d^4q}{i\pi^2} \left\{ \frac{\text{Tr} [L \not{p}_t \not{p}_d]}{\mathcal{A}_k^1 \mathcal{A}_k^2 \mathcal{A}_k^3 \mathcal{A}_k^4} \right\} \right), \quad (42)$$

$$\mathcal{B}_{k=g,h}^2(\hat{s}, \hat{t}) = -2m_t \hat{u} \text{Im} \left(\mathcal{X}_k'^R \mathcal{Y}_k^L \right) \text{Im} \left(\int \frac{d^4q}{i\pi^2} \left\{ \frac{\text{Tr} [L \not{q} \not{p}_d]}{\mathcal{A}_k^1 \mathcal{A}_k^2 \mathcal{A}_k^3 \mathcal{A}_k^4} \right\} \right). \quad (43)$$

Eqs. 40–43 then give:

$$\mathcal{B}_e^1(\hat{s}, \hat{t}) = -2Xm_t m_{\tilde{\chi}_n^0} \mathcal{O}_e^1 (D_0^e + D_{11}^e) , \quad (44)$$

$$\begin{aligned} \mathcal{B}_e^2(\hat{s}, \hat{t}) &= 2\mathcal{O}_e^2 \left\{ X m_t^2 D_{12}^e + \left[\hat{u}(\hat{u} - m_t^2)(\hat{s} - m_t^2) - m_t^2 \hat{u} \hat{t} \right] D_{24}^e \right. \\ &\quad + X(\hat{u} - m_t^2) D_{25}^e + 2\hat{u}(\hat{u} - m_t^2) D_{27}^e \\ &\quad + (\hat{u} - m_t^2) \left[m_t^2 \hat{u} D_{11}^e + \hat{u}(\hat{s} - m_t^2) D_{12}^e + X D_{13}^e \right] \\ &\quad \left. + m_t^2 \left[(X - \hat{u}(\hat{u} - m_t^2)) D_{11}^e - \hat{u} \hat{t} D_{12}^e \right] \right\} , \quad (45) \end{aligned}$$

$$\mathcal{B}_f^1(\hat{s}, \hat{t}) = \mathcal{B}_e^1(\hat{s}, \hat{t}) \left(m_{\tilde{\chi}_n^0} \rightarrow m_{\tilde{\chi}_m}, D_{ij}^e \rightarrow D_{ij}^f, \mathcal{O}_e^1 \rightarrow \mathcal{O}_f^1 \right) , \quad (46)$$

$$\mathcal{B}_f^2(\hat{s}, \hat{t}) = 0 , \quad (47)$$

$$\mathcal{B}_g^1(\hat{s}, \hat{t}) = 2m_{\tilde{\chi}_n^0} m_{\tilde{\chi}_m} \hat{u}(\hat{u} - m_t^2) \mathcal{O}_g^1 D_0^g , \quad (48)$$

$$\mathcal{B}_g^2(\hat{s}, \hat{t}) = -2m_t m_{\tilde{\chi}_m} \hat{u} \mathcal{O}_g^2 \left[(\hat{u} - m_t^2) D_{11}^g + \hat{t} D_{12}^e + \hat{s} D_{13}^e \right] , \quad (49)$$

$$\mathcal{B}_h^1(\hat{s}, \hat{t}) = \mathcal{B}_g^1(\hat{s}, \hat{t}) \left(D_0^g \rightarrow D_0^h, \mathcal{O}_g^1 \rightarrow \mathcal{O}_h^1 \right) , \quad (50)$$

$$\mathcal{B}_h^2(\hat{s}, \hat{t}) = \mathcal{B}_g^2(\hat{s}, \hat{t}) \left(m_{\tilde{\chi}_m} \rightarrow m_{\tilde{\chi}_n^0}, D_{ij}^g \rightarrow D_{ij}^h, \mathcal{O}_g^2 \rightarrow \mathcal{O}_h^2 \right) . \quad (51)$$

The SUSY CP-weak phases associated with the box diagrams, the \mathcal{O}_k^i 's above, are also given in appendix B and the corresponding four point one-loop form factors D_0^k, D_{pq}^k ($p = 1, 2$ and $q = 1 - 7$) are defined and given in appendix C.

PRA From The Decay Amplitude - A_D :

As mentioned before, there are four potential diagrams that can give rise to CP-violating PRA in the decay $t \rightarrow W^+ b$ within the MSSM. These are diagrams a-d in Fig. 2 where it should be understood that the t and W^+ momenta are reversed and the ud current is disregarded. It is convenient to denote these one-loop top decay diagrams with the same alphabetical order, i.e., a, b, c and d , similar to the corresponding production diagrams, as the SUSY CP-odd phases defined in Eqs. 22-29, the $\mathcal{O}_{a,b,c,d}^i$'s, are the same for both production and decay of the top.

We parameterize the $t \rightarrow W^+ b$ and $\bar{t} \rightarrow W^- \bar{b}$ decay vertices as follows:

$$J_k^{\mu(t)} \equiv i \frac{g_W}{\sqrt{2}} \sum_{P=L,R} \bar{u}_b \left(\frac{\mathcal{D}_{1(k)}^P p_t^\mu}{m_t} + \mathcal{D}_{2(k)}^P \gamma^\mu \right) P u_t , \quad (52)$$

$$J_k^{\mu(\bar{t})} \equiv i \frac{g_W}{\sqrt{2}} \sum_{P=L,R} \bar{v}_t \left(\frac{\bar{\mathcal{D}}_{1(k)}^P p_t^\mu}{m_t} + \bar{\mathcal{D}}_{2(k)}^P \gamma^\mu \right) P v_b , \quad (53)$$

Similar to the production process discussed above, $\mathcal{D}_{1(k)}^{L,R}$ and $\mathcal{D}_{2(k)}^{L,R}$ defined in Eqs. 52 and 53, contain the CP-violating odd phase as well as the absorptive phases of the decay diagram k , $k = a, b, c$ and d . Then, in terms of the scalar ($\mathcal{D}_{1(k)}$) and vector ($\mathcal{D}_{2(k)}$) form factors, the PRA, A_D , for the decay process is given by:

$$A_D = \sum_k \left\{ \frac{(x-1)}{2(x+2)} \text{Re}(\mathcal{D}_{1(k)}^R + \bar{\mathcal{D}}_{1(k)}^L) + \text{Re}(\mathcal{D}_{2(k)}^L - \bar{\mathcal{D}}_{2(k)}^L) \right\}. \quad (54)$$

Now $x \equiv m_t^2/m_W^2$ and the sum is carried out over all decay diagrams in Fig. 2 (i.e., $k = a, b, c$ and d). The relations between $\mathcal{D}_{1(k)}^R$ and $\bar{\mathcal{D}}_{1(k)}^L$ and between $\mathcal{D}_{2(k)}^L$ and $\bar{\mathcal{D}}_{2(k)}^L$ are the same as the relation between $\mathcal{P}_{1(k)}^L$ and $\bar{\mathcal{P}}_{1(k)}^R$ and between $\mathcal{P}_{2(k)}^L$ and $\bar{\mathcal{P}}_{2(k)}^L$, respectively, as is given in Eqs. 18–21.

For the scalar form factors in Eq. 54 we get:

$$\text{Re}(\mathcal{D}_{1(a)}^R + \bar{\mathcal{D}}_{1(a)}^L) = -\frac{8}{3} \frac{\alpha_s}{\pi} m_t m_{\tilde{g}} \mathcal{O}_a^1 C_{12}^a, \quad (55)$$

$$\text{Re}(\mathcal{D}_{1(b)}^R + \bar{\mathcal{D}}_{1(b)}^L) = -\frac{\alpha}{\pi \sin^2 \theta_W} m_t \left[m_t \mathcal{O}_b^1 (C_{22}^b - C_{23}^b) + m_{\tilde{\chi}_n^0} \mathcal{O}_b^2 C_{12}^b \right], \quad (56)$$

$$\begin{aligned} \text{Re}(\mathcal{D}_{1(c)}^R + \bar{\mathcal{D}}_{1(c)}^L) &= \frac{\alpha}{\pi \sin^2 \theta_W} m_t \left[m_t \mathcal{O}_c^1 (C_{23}^c - C_{22}^c) - m_{\tilde{\chi}_m} \mathcal{O}_c^2 (C_{11}^c - C_{12}^c) \right. \\ &\quad \left. + m_{\tilde{\chi}_n^0} \mathcal{O}_c^3 (C_0^c + C_{11}^c) \right], \end{aligned} \quad (57)$$

$$\text{Re}(\mathcal{D}_{1(d)}^R + \bar{\mathcal{D}}_{1(d)}^L) = \text{Re}(\mathcal{D}_{1(c)}^R + \bar{\mathcal{D}}_{1(c)}^L) \left(m_{\tilde{\chi}_n^0} \rightarrow -m_{\tilde{\chi}_m}, m_{\tilde{\chi}_m} \rightarrow m_{\tilde{\chi}_n^0}, \mathcal{O}_c^i \rightarrow \mathcal{O}_d^i, C_{ij}^c \rightarrow C_{ij}^d \right), \quad (58)$$

while the vector form factors in Eq. 54 are given by:

$$\text{Re}(\mathcal{D}_{2(a)}^L - \bar{\mathcal{D}}_{2(a)}^L) = 0, \quad (59)$$

$$\text{Re}(\mathcal{D}_{2(b)}^L - \bar{\mathcal{D}}_{2(b)}^L) = -\frac{\alpha}{\pi \sin^2 \theta_W} \mathcal{O}_b^1 C_{24}^b, \quad (60)$$

$$\begin{aligned} \text{Re}(\mathcal{D}_{2(c)}^L - \bar{\mathcal{D}}_{2(c)}^L) &= \frac{1}{2} \frac{\alpha}{\pi \sin^2 \theta_W} \left[\mathcal{O}_c^1 \left(m_t^2 (C_{22}^c - C_{23}^c) + m_W^2 (C_{11}^c + C_{22}^c - C_{12}^c - C_{23}^c) + 2C_{24}^c \right) \right. \\ &\quad \left. + m_t m_{\tilde{\chi}_m} \mathcal{O}_c^2 (C_{11}^c - C_{12}^c) - m_t m_{\tilde{\chi}_n^0} \mathcal{O}_c^3 (C_0^c + C_{11}^c - C_{12}^c) \right. \\ &\quad \left. - m_{\tilde{\chi}_m} m_{\tilde{\chi}_n^0} \mathcal{O}_c^4 C_0^c \right], \end{aligned} \quad (61)$$

$$\text{Re}(\mathcal{D}_{2(d)}^L - \bar{\mathcal{D}}_{2(d)}^L) = \text{Re}(\mathcal{D}_{2(c)}^L - \bar{\mathcal{D}}_{2(c)}^L) \left(m_{\tilde{\chi}_n^0} \rightarrow -m_{\tilde{\chi}_m}, m_{\tilde{\chi}_m} \rightarrow m_{\tilde{\chi}_n^0}, \mathcal{O}_c^i \rightarrow \mathcal{O}_d^i, C_{ij}^c \rightarrow C_{ij}^d \right). \quad (62)$$

As mentioned above, the SUSY CP-weak phases for the decay diagrams, the \mathcal{O}_k^i 's above, are the same as those for the production triangle diagrams a – d in Fig. 2 and are given in appendix B. Although the same notation (as in the production case) for the corresponding loop form factors C_0^k, C_{pq}^k is used

in the decay case at hand, these form factors are separately defined and given in appendix C.

4. CP Phases of The Low Energy MSSM and the Neutron EDM

Before presenting our numerical results, we wish to clarify our approach with regard to the CP-violating sector of the low energy MSSM and their effect on the NEDM. Disregarding for now the possible phases at the GUT scale, we assume for simplicity that at the EW scale, all CP-violation (apart from the usual SM phases) resides in the complex trilinear soft breaking terms, the A_f 's. For definiteness, we assume $\arg(\mu) = 0$ motivated by analyzing the NEDM, which suggests that $\arg(\mu) < \mathcal{O}(10^{-2})$ is required for the NEDM to satisfy the experimental bound for squark masses of a few hundred GeV (which we are assuming throughout the paper) [4, 5, 6, 7].

In fact, from a phenomenological point of view, this is certainly a plausible scenario that can emanate from a GUT-scale SUSY model in which the universality of the A terms is relaxed to give arbitrary phases $\arg(A_f^G)$ at the GUT-scale. In this regard, we take note of a recent very interesting work by Garisto and Wells [5]. They obtained severe constraints on the low energy phases of A_t and μ by deriving relations between the two. For that they use the complete set of RGE involving the complex parameters of a GUT-scale SUSY model with and without universal A terms and with some definite boundary conditions at the GUT-scale (for example $\arg(\mu^G) = \arg(A_f^G) = 0$). However, taking non-zero phases at the GUT-scale, the constraints obtained in [5] may not hold as, in general, assuming arbitrary phases at the GUT-scale one can practically make no prediction on the corresponding phases at the EW-scale. Our approach, the EW \rightarrow GUT approach, will be to assume a set of SUSY phases at the EW-scale, subject to existing experimental data, which implicitly assumes arbitrary phases at the scale in which the soft breaking terms are generated. With only the low energy phases of the various A_f terms, if all the squark masses except for the stops are degenerate with a mass M_s , then only $\arg(A_t)$ contributes to CP-violation in the reaction $p\bar{p} \rightarrow t\bar{b} + X \rightarrow W^+ b\bar{b} + X$. Any CP-odd phase from the trilinear soft breaking terms of the other squarks will enter into the asymmetry A , defined in Eq. 9, with a suppression factor of m_q^2/m_t^2 (q stands for any quark but the top) even if the squarks masses were not taken exactly degenerate. One power of m_q/m_t comes from the Dirac algebra when evaluating the squared matrix elements, if m_q is not neglected. Another m_q/m_t comes from the squarks mixing matrices: as can be seen from appendix A. The CP-violating quantity that arises from $\tilde{q}_L - \tilde{q}_R$ mixing (i.e., $\text{Im}(Z_q^{1i*} Z_q^{2i})$) is proportional to the SM quark masses, thus for $m_q/A_q \rightarrow 0$ there will be no mixing in the sector of the supersymmetric partners of the light quarks.

In appendix A we list the Feynman rules needed for calculating the CP-odd effect in the reaction $u\bar{d} \rightarrow t\bar{b} \rightarrow W^+b\bar{b}$. It is then obvious, that in principle, all the CP-violating vertices of the MSSM arise from diagonalization of the complex mass matrices Z_u , Z_d , Z_N , Z^- and Z^+ . However, with the assumption of $\arg(\mu) = 0$, it turns out that Z_N , Z^- and Z^+ are real. In particular, assuming the universality of the gaugino masses at the GUT-scale, the phase of the common gaugino mass, $\arg(M_{1/2})$, can be set to zero by a phase rotation [21], thus leaving the \tilde{m}_i $i = 1 - 3$ “phaseless” at any scale. We therefore have all CP-violation arising from $\tilde{t}_L - \tilde{t}_R$ mixing (i.e., from $\arg(A_t)$); in particular from (see appendix A):

$$\text{Im}(\xi_t^i) \equiv \text{Im}(Z_t^{1i*} Z_t^{2i}) = \frac{(-1)^{i-1}}{2} \sin 2\theta_t \sin \beta_t . \quad (63)$$

We will choose maximal CP-violation in the sense that $\text{Im}(\xi_t^i) = (-1)^{i-1}/2$ thus presenting all our numerical results in units of $\sin 2\theta_t \sin \beta_t$. With no further assumptions, what is left to be considered is the NEDM for a chosen set of the free parameters of the above phenomenological low energy MSSM.

The EDM of the neutron, d_n , is presumably one of the most important phenomenological problems associated with SUSY models especially with regard to CP violation. With a low energy MSSM that originates from a GUT-scale SUGRA model (with complete universality of the soft breaking terms), keeping d_n within its allowed experimental value (i.e., $d_n \leq 1.1 \times 10^{-25}$ e-cm [3]) requires the “fine tuning” of the SUSY phases to be less than or of the order of $10^{-2} - 10^{-3}$ for SUSY particle masses at around several hundred GeV’s [5].

When $\arg(\mu) = 0$, the leading contribution to a light quark EDM comes from gluino exchange, which, with the approximation of degenerate \tilde{u} and \tilde{d} squark masses (which we will denote by $m_{\tilde{q}}$), can be written as [5, 7]:

$$d_q(G) = \frac{2\alpha_s}{3\pi} Q_q e m_q \frac{|A_q| \sin \alpha_q}{m_{\tilde{q}}^3} \sqrt{r} K(r) , \quad (64)$$

where $m_q(m_{\tilde{q}})$ is the quark(squark) mass and Q_q is its charge. Also, $r \equiv m_G^2/m_{\tilde{q}}^2$ and $K(r)$ is given by [7, 22]:

$$K(r) = \frac{1}{(r-1)^3} \left(\frac{1}{2} + \frac{5}{2}r + \frac{r(2+r)}{1-r} \ln r \right) . \quad (65)$$

A_q is the complex trilinear soft breaking term at the EW scale associated with the squark \tilde{q} , and we have defined $A_q = |A_q|e^{i\alpha_q}$. Then, within the naive Quark Model, the NEDM can be obtained by relating it to the u and d quarks EDMs (i.e., d_u and d_d , respectively) by $d_n = (4d_d - d_u)/3$.

We stress again that with no universal boundary conditions for the soft trilinear terms and their phases at the GUT scale (i.e., $\arg(A_U) = \arg(A_D) = \arg(A_E) = \arg(A^G)$), there is no *a-priori* reason to believe that the low energy phases associated with the different A_f soft breaking terms are related at the EW scale. We therefore consider $\arg(A_u)$ and $\arg(A_d)$ to be free parameters of the model no matter what $\arg(A_t)$ is. In Figs. 3a and 3b we have plotted the allowed regions in the $\sin \alpha_u - \sin \alpha_d$ plane for $|d_n|$ not to exceed 1.1×10^{-25} e-cm (the present experimental limit) and 3×10^{-25} e-cm, respectively. In calculating d_n we assumed that the above naive Quark Model relation holds. Although there is no doubt that it can serve as a good approximation for an order of magnitude estimate it may still deviate from the true theoretical value which involves uncertainties in the calculation of the corresponding hadronic matrix elements (see [6] and references therein). Note also that it was recently argued that the naive quark model overestimates the NEDM, as the strange quark may carry an appreciable fraction of the neutron spin which can partly screen the contributions to the NEDM coming from the u and the d quarks [10]. To be on the safe side, we therefore slightly relax the theoretical limit on d_n in Fig. 3b to be 3×10^{-25} e-cm.

We have used, for these plots, $m_{\bar{d}} = m_{\bar{u}} = M_s = 400$ GeV, $m_G = 500$ GeV and for simplicity we also took $|A_u| = |A_d| = M_s$ (M_s is the only high SUSY mass scale associated with the squarks sector in our low energy MSSM. Therefore it is only natural to choose the mass scale of the soft breaking terms according to M_s). Also, we took the current quarks masses as $m_d = 10$ MeV, $m_u = 5$ MeV and $\alpha_s(m_Z) = 0.118$.

From Fig. 3a and in particular Fig. 3b, it is evident that $M_s = 400$ GeV and $m_G = 500$ GeV can be safely assumed, leaving “enough room” in the $\sin \alpha_u - \sin \alpha_d$ plane for $|d_n|$ not to exceed $1.1 - 3 \times 10^{-25}$ e-cm. In particular, while $\sin \alpha_u$ is basically not constrained, depending on $\sin \alpha_d$, $-0.35 \lesssim \sin \alpha_d \lesssim 0.35$ is needed for $|d_n| < 1.1 \times 10^{-25}$ e-cm and $-0.55 \lesssim \sin \alpha_d \lesssim 0.55$ is needed for $|d_n| < 3 \times 10^{-25}$ e-cm. Moreover, varying m_G between 250 GeV to 650 GeV (we will vary m_G in this range when discussing the numerical results below) almost has no effect on the allowed areas in the $\sin \alpha_u - \sin \alpha_d$ plane that are shown in Figs. 3a and 3b. That is, keeping $M_s = 400$ GeV and lowering m_G down to 250 GeV, very slightly shrinks the dark areas in Figs. 3a and 3b, whereas, increasing m_G up to 650 GeV slightly widens them. Of course, d_n strongly depends on the scalar mass M_s - increasing M_s enlarges the allowed regions in Figs. 3a and 3b as expected from Eq. 64. It is also very interesting to note from Fig. 3a that, in some instances, for a cancellation between the u and d quarks contributions to apply, $\sin \alpha_u, \sin \alpha_d > 0.1$ is essential rather than being just possible. For example, with $|\sin \alpha_u| \gtrsim 0.75$, $|\sin \alpha_d| \gtrsim 0.1$ is required in order to keep d_n below its experimental limit.

We can therefore conclude that CP-odd phases in the A terms at the order of $\text{few} \times 10^{-1}$ can be accommodated without too much difficulty with the existing experimental constraint on the NEDM even for typical SUSY masses of $\lesssim 500$ GeV. Therefore, somewhat in contrast to the commonly held viewpoint we do not find that a “fine-tuning” at the level of 10^{-2} is necessarily required for the SUSY CP-phases nor for the squark masses.

5. Numerical Results

We now turn to the discussion of our main numerical results. We first focus on CP-violating effects in the production amplitude which gives rise to the cross-section asymmetry, A_P , and then we will present our results for the PRA, A_D , associated with the top decay $t \rightarrow W^+ b$ and its conjugate one. Instead of using the asymmetry A_P defined in Eq. 9, after folding in the parton luminosities in the usual manner (see [19]), we define a Partially Integrated Cross-section Asymmetry (PICA) with respect to the variable τ or equivalently to \hat{s} ($\hat{s} = \tau s$). Thus:

$$A_P^{\text{PICA}} \equiv \frac{\int_{\tau_-}^{\tau_+} \left[\frac{d\mathcal{L}_{ud}(\tau)}{d\tau} \left(\hat{\sigma}(\hat{s} = \tau s) - \hat{\bar{\sigma}}(\hat{s} = \tau s) \right) \right] d\tau}{\int_{\tau_-}^{\tau_+} \left[\frac{d\mathcal{L}_{ud}(\tau)}{d\tau} \left(\hat{\sigma}(\hat{s} = \tau s) + \hat{\bar{\sigma}}(\hat{s} = \tau s) \right) \right] d\tau}, \quad (66)$$

where we have introduced the “parton luminosity” $d\mathcal{L}_{ud}(\tau)/d\tau$ [19]. We also define the invariant mass of the $t\bar{b}$ system to be $m_{t\bar{b}} \equiv \sqrt{\hat{s}}$. Then, in the numerical evaluation of the asymmetry A_P^{PICA} we choose τ_- and τ_+ according to $m_{t\bar{b}}^- = m_t$ ($m_b = 0$ is assumed through out the paper) and $m_{t\bar{b}}^+ = 350$ GeV, respectively. In the Tevatron, one of the problematic “backgrounds” to the reaction $p\bar{p} \rightarrow t\bar{b} + X$ is $t\bar{t}$ production [23]. In principle, the $t\bar{t}$ background can be eliminated by imposing the above naive upper cut on $m_{t\bar{b}}$, which is below the $t\bar{t}$ production threshold (i.e., $m_{t\bar{b}}^+ = 350$ GeV $\lesssim 2m_t$). Although the actual experimental cuts that will be made in order to remove the $t\bar{t}$ “background” in the Tevatron (when studying the $t\bar{b}$ final state) might be more involved, this naive cut on $m_{t\bar{b}}$ serves our purpose. A detailed discussion of the exact experimental cuts for the $t\bar{b}$ final state is beyond the scope of this paper but can be found in [1, 23]. Note also that this upper cut on $m_{t\bar{b}}$ has practically no effect on the cross-section for $p\bar{p} \rightarrow t\bar{b} + X$ (or equivalently the available number of $t\bar{b}$ events in the future 2 TeV Tevatron), as most of the $t\bar{b}$ pairs will be produced with an invariant mass of $m_{t\bar{b}} \lesssim 350$ GeV. In particular, the fully integrated cross-section for $p\bar{p} \rightarrow t\bar{b} + X$ is (i.e., up to $m_{t\bar{b}} = 2$ TeV)

$\sigma(s = 2 \text{ TeV}) \approx 360 \text{ [fb]}$ [1], out of which $\sim 80\%$ of the $t\bar{b}$ pairs are produced with an invariant mass $m_{t\bar{b}} \lesssim 350 \text{ GeV}$.

For the numerical evaluation of the CP-violating asymmetry A_P^{PICA} , we take $M_s = 400 \text{ GeV}$. We also vary the gluino mass between $250 \text{ GeV} < m_G < 650 \text{ GeV}$ (as was emphasized in the previous section, these masses of the degenerate squarks and the gluino do not contradict the existing experimental upper limit on the NEDM). We choose two representative values for $\tan\beta$; $\tan\beta = 1.5$ and $\tan\beta = 35$ which correspond to a low and a high $\tan\beta$ scenario, respectively. The low energy Higgs mass parameter μ is varied between -400 to $+400 \text{ GeV}$, whereas, the mass of the light stop (m_t) is varied between 50 to 400 GeV . As mentioned above, we also choose maximal CP-violation, driven by $\tilde{t}_L - \tilde{t}_R$ mixing, in the sense that $\xi_t^i = (-1)^{1-i}/2$ (see Eq. 63), whereas, we take $\arg(\mu) = 0$. Therefore the asymmetries are always given in units of $\sin 2\theta_t \sin\beta_t$.

The consequences of this low energy MSSM scenario (with the above chosen mass spectrum and CP-odd phases) with regard to the various diagrams that are depicted in Fig. 2 are:

- I) The triangle diagrams $2c, 2b', 2c'$ and $2d'$ as well as the box diagrams $2f$ and $2h$ do not acquire any CP-violating phase in the limit $\arg(\mu) = 0$.
- II) Diagram $2a'$ does not have any CP-violating phase in the limit $m_u, m_d \rightarrow 0$.
- III) Diagram $2a$ does not have an absorptive cut for $m_{t\bar{b}} < 350 \text{ GeV}$.
- IV) Diagram $2b$ is p -wave suppressed near threshold. Thus its contribution to A_P^{PICA} is negligible compared to the other diagrams.

With the above points I–IV, the study of CP-violation in this reaction simplifies to a large extent. That is, we are left with only three CP-violating diagrams that can make important contributions to A_P^{PICA} . These are: diagram $2d, 2e$ and $2g$ out of which diagram $2d$ is expected to be the most important one. In particular, in the range where the asymmetry exceeds the 1% level, diagram $2d$ is responsible for $\sim 90\%$ of the total CP-odd effect in A_P^{PICA} . Moreover, it is important to note that while the CP-violating effects from diagrams $2e$ and $2g$ strongly depend on the heavy scalars mass M_s (through two scalar exchanges in the loop), diagram $2d$ is less sensitive to M_s having only one scalar exchange in the loop. In particular, as M_s increases, diagram $2d$ becomes relatively more dominant as far as CP is concerned (Of course, in general, increasing the SUSY scale M_s causes the asymmetry to drop for diagrams $2d$ as well as for diagrams $2e$ and $2g$). It is worth mentioning that, in that range where the asymmetry is above the percent level mainly due to the CP-effects coming from diagram $2d$, the CP-violating effect driven by diagrams $2e$ and $2g$ has the same relative sign to that of diagram $2d$, thus yielding a slightly bigger overall asymmetry. Nonetheless, for simplicity, we

will present all our numerical results only for diagram 2d. In any case, we are only interested in a rough estimate of the CP-violating effect in the reaction $p\bar{p} \rightarrow t\bar{b} + X$ and not in the exact numbers, as many simplifying assumptions had to be made along the way.

In Figs. 4a and 4b we have plotted A_P^{PICA} for $M_s = 400$ GeV, $m_l = 50$ GeV and for three values of m_G as a function of the low energy Higgs mass parameter μ , for $\tan\beta = 1.5$ and $\tan\beta = 35$, respectively [24, 25]. We see from Fig. 4a that in the low $\tan\beta$ scenario and a gluino mass between $350 \text{ GeV} \lesssim m_G \lesssim 550 \text{ GeV}$, moderately negative values of μ , lying in a narrow range, $-100 \text{ GeV} \lesssim \mu \lesssim -70 \text{ GeV}$, are required for the asymmetry to be above 2%. In the best case, for $m_G = 450$ GeV the asymmetry peaks at around $\mu \approx -90$ GeV, reaching $\sim 2.75\%$. A positive μ around 140(240) GeV may also give rise to a $\sim 2(1)\%$ asymmetry for a gluino mass $m_G \approx 550$ GeV. Also, for $\mu \lesssim -200$ GeV and $\mu \gtrsim 350$ GeV the asymmetry drops below the 0.25% level. From Fig. 4b (high $\tan(\beta)$) we see that around $|\mu| \sim 110$ GeV the asymmetry can also reach the 2% level for $400 \text{ GeV} \lesssim m_G \lesssim 575 \text{ GeV}$ (see also Fig. 6b). Here, the asymmetry drops below the 0.25% level for $|\mu| \gtrsim 250$ GeV. Notice that, in the high $\tan\beta$ scenario, A_P^{PICA} is almost insensitive to the sign of μ . This happens mainly due to the fact that, for high values of $\tan\beta$, the charginos and neutralinos masses are almost independent of the sign of μ as can be also seen in Table 1. The only terms in the chargino and neutralino masses which linearly depend on μ are proportional to $\sin 2\beta$ which is of the order of $\text{few} \times 10^{-2}$ for $\tan\beta \gtrsim 30$ (see Eq. A.22 and A.25–A.32).

Before discussing the results in Figs. 5–11 we remark that, in what follows, we choose several representative values of μ ; some of them maximize CP-effect in the production amplitude and some maximize the CP-violating PRA effect in the decay $t \rightarrow bW$ to be discussed later. In particular, for $\tan\beta = 1.5$ we always take the values $\mu = -70, -90, -130, 140$ and 240 GeV, while for $\tan\beta = 35$ we choose $\mu = -110, -170, -190, 110$ and 170 GeV, although, in some cases the combination of $\{\tan\beta, \mu, m_G\}$ for some of those values is forbidden according to our criteria (see section 2). It is useful to keep track of the charginos and neutralinos masses for a given set of $\{\tan\beta, \mu, m_G\}$, especially due to the various absorptive thresholds that can emanate from the loop integral of diagram 2d [25]. Therefore, for the reader's convenience, we give in Table 1 the masses of the charginos and neutralinos for various sets of $\{\tan\beta, \mu, m_G\}$ that are repeatedly being used throughout this analysis.

In Figs. 5a and 5b we show the dependence of A_P^{PICA} on m_l , the mass of the light stop, for various values of μ , $M_s = 400$ GeV and for $\tan\beta = 1.5$ and $\tan\beta = 35$, respectively. However, the general behavior that is depicted in Figs. 5a and 5b holds for any value of μ . That is, as expected, when m_l is increased the asymmetry falls till it totally vanishes for $m_l = 400$ GeV in which case the two stop species are degenerate. It is evident from Figs. 5a and 5b that, in general, $m_l \lesssim 75$ GeV is needed

for the asymmetry to be above $\sim 1\%$, although in some cases, for example when $\mu = -70$ GeV and $\tan\beta = 1.5$, a 1% asymmetry can arise even with $m_l \gtrsim 100$ GeV.

The dependence of A_P^{PICA} on the gluino mass m_G is shown in Figs. 6a and 6b for $\tan\beta = 1.5$ and $\tan\beta = 35$, respectively. Here again, we took $M_s = 400$ GeV and $m_l = 50$ GeV and choose the same representative values for μ . We see that for a small $\tan\beta$ and a negative μ around -100 GeV, $A_P^{\text{PICA}} \gtrsim 2.5\%$ for $350 \text{ GeV} \lesssim m_G \lesssim 550 \text{ GeV}$ and peaks at around $m_G \sim 400$ GeV. Note that even a heavy gluino, e.g., $m_G \approx 650$ GeV, can give rise to a $\gtrsim 2\%$ asymmetry if $\mu \approx -90$ GeV and $\tan\beta$ is of order one. We see from Fig. 6b that for large $\tan\beta$ and for $|\mu| = 110$ GeV, $A_P^{\text{PICA}} \sim 2\%$ for $400 \text{ GeV} \lesssim m_G \lesssim 550 \text{ GeV}$ and peaks at $m_G \sim 450$ GeV. In both the low and high $\tan\beta$ scenarios, with a “light” gluino, $m_G \lesssim 300$ GeV, the cross-section asymmetry is below 1%.

Figs. 7a and 7b show the dependence of A_P^{PICA} on $\tan\beta$ for $m_G = 350$ and 550 GeV, respectively. Evidently, as far as CP is concerned, a low $\tan\beta$ is better than a high one. We see that as one goes to $\tan\beta \gtrsim 10$, the asymmetry is almost insensitive to $\tan\beta$. This also holds for high values up to $\tan\beta = 65$ which are not shown in Figs. 7a and 7b.

Until now we were not interested in the overall sign of the cross-section asymmetry A_P^{PICA} . Including the PRA CP-violating effect, A_D , coming from the decaying top, the relative sign between A_P^{PICA} and A_D becomes important as the total CP-violating effect is the sum of the two i.e., $A = A_P^{\text{PICA}} + A_D$. However, we will show below that, in most instances, A_D is smaller than A_P^{PICA} by more than an order of magnitude and, therefore, its relevance to the CP-effect in $p\bar{p} \rightarrow t\bar{b} + X \rightarrow W^+ b\bar{b} + X$ is negligible.

Let us now discuss the PRA effect, A_D . Once again, we will use our low energy MSSM scenario (described in detail in section 2 and 4) to estimate the CP-odd effect. Although, as was mentioned before, the PRA A_D does not depend on the specific production mechanisms of the t and \bar{t} , in most cases we will evaluate its magnitude within the same ranges of the SUSY free parameter space as was taken in Figs. 4–7. This should enable the reader to easily extract the overall asymmetry emanating from both production and decay processes discussed in this paper. However, as was mentioned above, throughout most of the range of our SUSY parameter space, A_D is more than one order of magnitude smaller than A_P^{PICA} , therefore, the relative sign between A_D and A_P^{PICA} is essentially irrelevant. Note that the consequences of the low energy MSSM framework on the various diagrams (i.e., the “reversed” diagrams $a - d$ in Fig. 2) that can potentially contribute to A_D are:

- I) For $m_G > 250$ GeV diagram 2a does not have the needed absorptive cut and thus, does not contribute to A_D .
- II) As in the case of production, diagram 2c does not have a CP-violating phase in the limit $\arg(\mu) =$

0. We are therefore left with only two diagrams that can contribute to A_D . These are: diagram 2b and 2d, where the leading contribution to A_D again comes from diagram 2d.

Our main results for A_D are shown in Figs. 8–11. A quick look at Figs. 8–11 reveals that, throughout a large portion of the SUSY parameter space discussed here, A_D tends to be below 0.1%, although for some specific values of the parameters it can approach 0.3%. The asymmetry we find is therefore somewhat small compared to the estimates of Grzadkowski and Keung (GK) and of Christova and Fabbrichesi (CF) in [9]. In the GK limit only the gluino exchange of diagram 2a was considered in which case $m_G \lesssim 120$ GeV is required in order to have the necessary absorptive cut (when $m_t = 50$ GeV). In the best case, GK found a $\sim 1\%$ asymmetry for $m_G = m_{\tilde{t}} = 100$ GeV [26]. On the other hand, in the CF limit, numerical results were given only for the neutralino exchange diagram (i.e., diagram 2b) wherein the CP-phase was chosen to be proportional to $\arg(\mu)$ and maximal CP-violation with regard to $\arg(\mu)$ was taken [27]. In the best case, CF found a $\sim 2\%$ asymmetry for $m_{\tilde{t}} = 100$ GeV. However, each of those largish PRA asymmetries, reported by GK and CF in [9], suffer from two drawbacks. (i) For the GK limit, $m_G \lesssim 120$ GeV is now essentially disallowed by the current experimental bounds. (ii) For the CF limit, $\arg(\mu) \gtrsim 10^{-2}$ is an unnatural choice bearing the stringent constraints on this phase coming from the experimental limits on the NEDM as discussed in section 4. (iii) For both the GK and CF limits, the large asymmetry arises once the masses of the superpartners of the light quarks are set to 100 GeV. Again, this is a rather unnatural choice as it is theoretically very hard, if at all possible, to meet the NEDM experimental limits when the masses of the squarks (except for the lighter stop) are at the order of 100 GeV. Instead, we discuss below the PRA effect, A_D , including all possible diagrams and subject to the available experimental bounds on both the NEDM and the supersymmetric spectrum. In particular, we again take $\arg(\mu) = 0$, $m_{\tilde{q}} = M_s = 400$ GeV, $m_t > 50$ GeV, $m_G > 250$ GeV, the LSP mass to be above 20 GeV and the mass of the lighter chargino to be above 65 GeV (see sections 2 and 4) [24].

As can be seen from Figs. 8a, 9a and 10a, in the low $\tan\beta$ case (i.e., $\tan\beta = 1.5$) and for negative values of μ in the range -90 GeV $\lesssim \mu \lesssim -30$ GeV, A_D can be about 0.1–0.2% provided the gluino mass lies in the range 300 GeV $\lesssim m_G \lesssim 550$ GeV and the lighter stop mass (m_t) is between ~ 50 and ~ 70 GeV. In fact, A_D can even reach $\sim 0.3\%$ if in addition to m_t being in that narrow range we also have $m_G \approx 320$ GeV. As μ becomes positive, at $\mu \approx 150$ GeV, A_D tends to grow with the gluino mass. In particular, we find for example that for $\mu \approx 140$ GeV and $m_G \gtrsim 600$ GeV, $A_D \sim 0.2\%$ becomes possible. The results for the high $\tan\beta$ case (i.e., $\tan\beta = 35$) are shown in Figs. 8b, 9b and 10b. Evidently, with a high $\tan\beta$, $|A_D| < 0.1\%$ throughout all the range of our SUSY parameter space.

The dependence of A_D on the lighter stop mass, m_l , is shown in Figs. 9a and 9b. As expected, A_D drops as m_l is increased and vanishes for $m_l > m_t - m_{\text{LSP}}$ (m_{LSP} is the LSP mass), for which case there is no absorptive cut in any of the diagrams $a - d$ in Fig. 2 [25].

Finally, in Figs. 11a and 11b we evaluate A_D as a function of $\tan\beta$ for $m_G = 350$ and 550 GeV, respectively. We can see that, here also, a small $\tan\beta$ gives rise to a bigger asymmetry and, as $\tan\beta$ grows above ~ 10 , A_D becomes insensitive to it. In the best cases, for $\tan\beta \sim \mathcal{O}(1)$, $|A_D| \sim 0.3\%$ become possible for both $m_G = 350$ and 550 GeV.

Before summarizing, we wish to emphasize that the decay asymmetry A_D is independent of the production mechanism. Therefore, the LHC with its large ($\sim 10^7$) production rate for $t\bar{t}$ pairs could be a good place to search for A_D . To probe such a PRA signal in the top decay $t \rightarrow bW$, of the order of a few tenths of a percent, will naively require $\sim 10^6$ $t\bar{t}$ pairs when no efficiency factors are taken into account. Note that such a measurement requires only the detection of the charge of the top for which the systematic errors may be kept relatively small. Even if we take an efficiency overall factor of ~ 0.1 , then with $\sim 10^7$ $t\bar{t}$ pairs the reach of the LHC will be around $A_D \gtrsim 0.3\%$. Although, as we discussed in the preceding pages, in our SUSY study it appears difficult to attain that large a decay asymmetry, the experimental search would still be worthwhile.

6. Summary and Conclusions

To summarize, we found that within a portion of a plausible MSSM low energy parameter space, a CP-violating cross-section asymmetry in the reaction $p\bar{p} \rightarrow t\bar{b} + X$ can be at the level of a few percent. Furthermore, a CP-violating PRA effect in the subsequent top decay cannot exceed the 0.3% level throughout our chosen range of the MSSM free parameter space. Therefore, the CP-violating asymmetry in this reaction arises predominantly from the production vertex. These asymmetries, in production and decay of the top, are driven by the complex entry of the soft trilinear breaking term associated with the top, $\arg(A_t)$. In particular, we have shown that for scalar SUSY masses as well as a gluino mass of the order of 0.5 TeV, and with a Higgs mass parameter, μ , at the range of $-250 \text{ GeV} \lesssim \mu \lesssim 250 \text{ GeV}$ a CP-violating signal above the percent level might indeed arise in the reaction $p\bar{p} \rightarrow t\bar{b} + X \rightarrow W^+b\bar{b} + X$, provided that the light stop particle have a mass below 100 GeV.

We have also shown that this phenomenologically acceptable low energy MSSM scenario does not contradict the experimental limit on the NEDM (i.e., $d_n < 1.1 \times 10^{-25}$ e-cm). In particular, in our low energy MSSM framework, SUSY CP-odd phases in the trilinear soft breaking terms (A_f 's) at the order of $\text{few} \times 10^{-1}$ are allowed even with squark masses below 500 GeV. The theoretical

uncertainties involved in calculating the NEDM may even strengthen this statement. In this respect our findings are somewhat different from what is commonly claimed in the literature.

In the future 2 TeV $p\bar{p}$ Tevatron collider, the cross-section for $p\bar{p} \rightarrow t\bar{b} + X$ is expected to be about 300 (fb) if a cut of $m_{t\bar{b}} < 350$ GeV is applied on the invariant mass of the $t\bar{b}$. Therefore with an integrated luminosity of $\mathcal{L} = 30$ (fb) $^{-1}$ [1, 23] an asymmetry $A_{\text{PICA}} \sim 3\%$, which was found here in the best cases, can be naively detected with a statistical significance of 3σ . We must caution, however, that the values of the asymmetry as large as 3% appear attainable only for some specific range for some of the input parameters. Note also such a detection at the Tevatron will require the identification of all $t\bar{b}$ pairs, which, in principle, can be achieved only if the top can be reconstructed even when the W decays hadronically. Therefore, at the future 2 TeV $p\bar{p}$ collider, a percent level CP-violating signal in the reaction $p\bar{p} \rightarrow t\bar{b} + X \rightarrow W^+b\bar{b} + X$ may become accessible. We have also emphasized that the PRA effect in the decay $t \rightarrow bW$ may be measurable at the LHC.

Note that the above line of reasoning can be reversed. That is, one can ask: what limit can be obtained on $\arg(A_t)$ by studying CP-violation in the reaction $p\bar{p} \rightarrow t\bar{b} + X \rightarrow W^+b\bar{b} + X$ at the next runs of the Tevatron or in the decay $t \rightarrow bW$ at the LHC? We found that in the best case, the 2 TeV Tevatron with $\mathcal{L} = 30$ (fb) $^{-1}$ will be marginally sensitive to CP-odd effects coming from $\arg(A_t)$ and, taking into account the various efficiency factors for such a detection, perhaps a $\sim 1 - 2$ -sigma bound on $\arg(A_t)$ will be feasible. However, note that in a possible Tevatron upgrade with center of mass energy of 4 TeV [1], the production rate of $t\bar{b}$ becomes three times bigger and, therefore, in such an upgraded version of the Tevatron a more stringent upper limit may indeed be placed on $\arg(A_t)$ through the study of the $t\bar{b}$ cross-section as suggested here. The LHC may also be sensitive to $\arg(A_t)$ through a study of a PRA effect in the top decay $t \rightarrow bW$ if the SUSY parameter space lies in the window wherein the PRA effect reaches its maximum values i.e., 0.1–0.3%. In such a scenario a statistically significant limit on $\arg(A_t)$ may be within its reach.

In closing, we wish to remark that it will be useful to explore the SUSY mediated CP-violating effects that can emanate in the W -gluon fusion subprocess which contributes to the same final state (i.e., $Wg \rightarrow t\bar{b}d$) and which has a comparable production rate to that of the simple $u\bar{d} \rightarrow t\bar{b}$ in the 2 TeV Tevatron. Unlike in the case of the 2HDM [2], where, to one-loop order, no CP-violating corrections enter the W -gluon subprocess, within the MSSM, various one-loop triangle and box corrections can give rise to CP-nonconservation also in the W -gluon fusion subprocess. However, it is also important to emphasize that due to the extra light jet in $Wg \rightarrow t\bar{b}d$ and the different kinematics, in principle, the $t\bar{b}$ pairs originating from the W -gluon fusion can be distinguished from those produced via the $u\bar{d}$ fusion [28].

Acknowledgments

We thank Gad Eilam for discussion and advice. We must also thank Galit Eyal for checking many of the calculations. S.B. also thanks Ann Heinson for discussions. We acknowledge partial support from U.S. DOE contract numbers DE-AC02-76CH00016(BNL), DC-AC05-84ER40150(Jefferson Lab) and DE-FG03-94ER40837(UCR).

Appendix A

In this appendix we list the relevant pieces of the SUSY lagrangian written in terms of the mass eigenstates. We also give the analytical expressions for all the corresponding mass mixing matrices Z_f , Z_N , Z^+ , Z^- and the masses of the supersymmetric particles which are functions of these matrix elements.

The SUSY lagrangian pieces are [13]:

$$\mathcal{L}_{\tilde{u}_i \tilde{d}_j W} = -\frac{ig}{\sqrt{2}} Z_d^{1j} Z_u^{1i} V^{ud} (\tilde{d}_j^+ \overleftrightarrow{\partial}^\mu \tilde{u}_i^+) W_\mu^- + H.c. , \quad (\text{A.1})$$

$$\begin{aligned} \mathcal{L}_{\tilde{u}_i \tilde{d} \tilde{\chi}_m} = & \tilde{u}_i^+ \tilde{d}^- \left\{ \left[-g Z_u^{1i} Z_{1m}^{+*} + \frac{\sqrt{2} m_u}{v_2} Z_u^{2i} Z_{2m}^{+*} \right] R + \right. \\ & \left. \frac{\sqrt{2} m_d}{v_1} Z_u^{1i} Z_{2m}^- L \right\} V^{ud} \tilde{\chi}_m^c + H.c. , \end{aligned} \quad (\text{A.2})$$

$$\begin{aligned} \mathcal{L}_{\tilde{d}_j \tilde{u} \tilde{\chi}_m} = & -\tilde{d}_j^+ \tilde{\chi}_m^- \left\{ \left[g Z_d^{1j} Z_{1m}^- - \frac{\sqrt{2} m_d}{v_1} Z_d^{2j} Z_{2m}^- \right] L - \right. \\ & \left. \frac{\sqrt{2} m_u}{v_2} Z_d^{1j} Z_{2m}^{+*} R \right\} V^{ud} u + H.c. , \end{aligned} \quad (\text{A.3})$$

$$\begin{aligned} \mathcal{L}_{\tilde{u}_i \tilde{u} \tilde{\chi}_n^0} = & \tilde{u}_i^- \tilde{\chi}_n^0 \left\{ \left[-\frac{g}{\sqrt{2}} Z_u^{1i*} L^+ - \frac{\sqrt{2} m_u}{v_2} Z_u^{2i*} Z_N^{4n} \right] L + \right. \\ & \left. \left[\frac{2\sqrt{2}}{3} g \tan \theta_W Z_u^{2i*} Z_N^{1n*} - \frac{\sqrt{2} m_u}{v_2} Z_u^{1i*} Z_N^{4n*} \right] R \right\} u + H.c. , \end{aligned} \quad (\text{A.4})$$

$$\begin{aligned} \mathcal{L}_{\tilde{d}_j \tilde{d} \tilde{\chi}_n^0} = & \tilde{d}_j^+ \tilde{\chi}_n^0 \left\{ \left[-\frac{g}{\sqrt{2}} Z_d^{1j} L^- - \frac{\sqrt{2} m_d}{v_1} Z_d^{2j} Z_N^{3n} \right] L + \right. \\ & \left. \left[-\frac{\sqrt{2}}{3} g \tan \theta_W Z_d^{2j} Z_N^{1n*} - \frac{\sqrt{2} m_d}{v_1} Z_d^{1j} Z_N^{3n*} \right] R \right\} d + H.c. , \end{aligned} \quad (\text{A.5})$$

$$\mathcal{L}_{\tilde{u}_i \tilde{u} \tilde{g}} = \sqrt{2} g_s \tilde{u}_i^- T^a \tilde{g}^a \left[-Z_u^{1i*} L + Z_u^{2i*} R \right] u + H.c. , \quad (\text{A.6})$$

$$\mathcal{L}_{\tilde{d}_j \tilde{d} \tilde{g}} = \sqrt{2} g_s \tilde{d}_j^+ T^a \tilde{g}^a \left[-Z_d^{1j} L + Z_d^{2j} R \right] d + H.c. , \quad (\text{A.7})$$

$$\mathcal{L}_{W \tilde{\chi}_m \tilde{\chi}_n^0} = g \tilde{\chi}_m \gamma^\mu \left\{ K^- L + K^+ R \right\} \tilde{\chi}_n^0 W_\mu^+ + H.c. , \quad (\text{A.8})$$

where $L(R) = \frac{1}{2}(1 - (+)\gamma_5)$ and the \tilde{u}_i and u (\tilde{d}_j and d) stand for up squark and up quark (down squark and down quark), respectively. Also $\tilde{\chi}_m$, $\tilde{\chi}_n^0$ and \tilde{g} are the charginos, neutralinos and gluinos respectively. We have also defined:

$$L^\pm \equiv \frac{1}{3} \tan \theta_W Z_N^{1n} \pm Z_N^{2n} , \quad (\text{A.9})$$

$$K^+ \equiv Z_N^{2n*} Z_{1m}^- + \frac{1}{\sqrt{2}} Z_N^{3n*} Z_{2m}^- , \quad (\text{A.10})$$

$$K^- \equiv Z_N^{2n} Z_{1m}^{+*} - \frac{1}{\sqrt{2}} Z_N^{4n} Z_{2m}^{+*} , \quad (\text{A.11})$$

and the mixing matrices Z_u , Z_d , Z_N , Z^- and Z^+ are given below.

Let us define the following diagonalizing mass matrices [7, 12, 13, 17, 29, 30]:

$$Z_f^+ M_f^2 Z_f = \text{diag} (m_{f_1}^2, m_{f_2}^2) , \quad (\text{A.12})$$

$$(Z^-)^T M_{\tilde{\chi}} Z^+ = \text{diag} (m_{\tilde{\chi}_1}, m_{\tilde{\chi}_2}) , \quad (\text{A.13})$$

$$Z_N^T M_{\tilde{\chi}^0} Z_N = \text{diag} (m_{\tilde{\chi}_1^0}, m_{\tilde{\chi}_2^0}, m_{\tilde{\chi}_3^0}, m_{\tilde{\chi}_4^0}) , \quad (\text{A.14})$$

where M_f^2 is the mass squared matrix of the scalar partners of a fermion. $M_{\tilde{\chi}}$ and $M_{\tilde{\chi}^0}$ are the mass matrices of the charginos and neutralinos, respectively.

M_f^2 is then given by [7, 12, 13]:

$$M_f^2 = \begin{bmatrix} m_f^2 - \cos 2\beta (T_{3f} - Q_f \sin^2 \theta_W) M_Z^2 + m_{\tilde{f}_L}^2 & -m_f (R_f \mu + A_f^*) \\ -m_f (R_f \mu^* + A_f) & m_f^2 - \cos 2\beta Q_f \sin^2 \theta_W M_Z^2 + m_{\tilde{f}_R}^2 \end{bmatrix} , \quad (\text{A.15})$$

where m_f is the mass of the fermion f , Q_f its electric charge and T_{3f} the third component of the weak isospin of a left-handed fermion f . $m_{\tilde{f}_L}^2$ ($m_{\tilde{f}_R}^2$) is the low energy mass squared parameter for the left(right) sfermion \tilde{f}_L (\tilde{f}_R). $R_f = \cot \beta (\tan \beta)$ for $T_{3f} = \frac{1}{2} (-\frac{1}{2})$ where $\tan \beta = v_2/v_1$.

$M_{\tilde{\chi}}$ and $M_{\tilde{\chi}^0}$ are given by [7, 12, 13, 17, 30]:

$$M_{\tilde{\chi}} = \begin{bmatrix} \tilde{m}_2 & \sqrt{2} M_W \sin \beta \\ \sqrt{2} M_W \cos \beta & \mu \end{bmatrix} , \quad (\text{A.16})$$

$$M_{\tilde{\chi}^0} = \begin{bmatrix} \tilde{m}_1 & 0 & -M_Z \cos \beta \sin \theta_W & M_Z \sin \beta \sin \theta_W \\ 0 & \tilde{m}_2 & M_Z \cos \beta \cos \theta_W & -M_Z \sin \beta \cos \theta_W \\ -M_Z \cos \beta \sin \theta_W & M_Z \cos \beta \cos \theta_W & 0 & -\mu \\ M_Z \sin \beta \sin \theta_W & -M_Z \sin \beta \cos \theta_W & -\mu & 0 \end{bmatrix} , \quad (\text{A.17})$$

where \tilde{m}_1 (\tilde{m}_2) is the mass parameter for the $U(1)$ ($SU(2)$) gaugino.

After diagonalizing these mass matrices according to Eq. A.12–A.14, the corresponding masses of the supersymmetric partners of the fermions, the charginos and the neutralinos are given by:

$$M_{\tilde{f}_1(\tilde{f}_2)}^2 = \frac{a_f - (+)\sqrt{b_f^2 + c_f^2}}{2}, \quad (\text{A.18})$$

$$a_f = 2m_f^2 - \cos 2\beta T_{3f} M_Z^2 + m_{\tilde{f}_L}^2 + m_{\tilde{f}_R}^2, \quad (\text{A.19})$$

$$b_f = \cos 2\beta (2Q_f \sin^2 \theta_W - T_{3f}) M_Z^2 + m_{\tilde{f}_L}^2 - m_{\tilde{f}_R}^2, \quad (\text{A.20})$$

$$c_f = -2m_f \left| R_f \mu + A_f^* \right|, \quad (\text{A.21})$$

$$M_{\tilde{\chi}_1(\tilde{\chi}_2)}^2 = \frac{1}{2} \left[\tilde{m}_2^2 + \mu^2 + 2M_W^2 - (+) \left[(\tilde{m}_2^2 - \mu^2)^2 + 4M_W^4 \cos^2 2\beta + 4M_W^2 (\tilde{m}_2^2 + \mu^2 + 2\tilde{m}_2 \mu \sin 2\beta) \right]^{\frac{1}{2}} \right]. \quad (\text{A.22})$$

In Eq. A.14 we have defined Z_N such that the elements of the diagonal neutralinos mass matrix are real and non-negative. It is sometimes more convenient to allow for negative entries for the $m_{\tilde{\chi}_i^0}$ which implies the change of Eq. A.14 to [29, 30]:

$$NM_{\tilde{\chi}_0} N^{-1} = \text{diag}(\epsilon_1 m_{\tilde{\chi}_1^0}, \epsilon_2 m_{\tilde{\chi}_2^0}, \epsilon_3 m_{\tilde{\chi}_3^0}, \epsilon_4 m_{\tilde{\chi}_4^0}), \quad (\text{A.23})$$

where N is a real matrix. While the $m_{\tilde{\chi}_i^0}$ are always positive, the ϵ_i 's are either ± 1 . With this substitution, in the Feynman rules one has to use the relation [29, 30] (note the slight difference between our notation for Z_N and the one used in [29]):

$$Z_{Nij} = \left(\sqrt{\epsilon_j} \right)^* N_{ji}, \quad (\text{A.24})$$

The positive real masses of the neutralinos are then given by:

$$\epsilon_1 m_{\tilde{\chi}_1^0} = -a_{\tilde{\chi}} + \sqrt{b_{\tilde{\chi}} + c_{\tilde{\chi}}} + d_{\tilde{\chi}}, \quad (\text{A.25})$$

$$\epsilon_2 m_{\tilde{\chi}_2^0} = a_{\tilde{\chi}} - \sqrt{b_{\tilde{\chi}} - c_{\tilde{\chi}}} + d_{\tilde{\chi}}, \quad (\text{A.26})$$

$$\epsilon_3 m_{\tilde{\chi}_3^0} = -a_{\tilde{\chi}} - \sqrt{b_{\tilde{\chi}} + c_{\tilde{\chi}}} + d_{\tilde{\chi}}, \quad (\text{A.27})$$

$$\epsilon_4 m_{\tilde{\chi}_4^0} = a_{\tilde{\chi}} + \sqrt{b_{\tilde{\chi}} - c_{\tilde{\chi}}} + d_{\tilde{\chi}}, \quad (\text{A.28})$$

where:

$$a_{\tilde{\chi}} = \left(\frac{1}{2}a - \frac{1}{6}C_2 \right)^{\frac{1}{2}}, \quad (\text{A.29})$$

$$b_{\tilde{\chi}} = -\frac{1}{2}a - \frac{1}{3}C_2, \quad (\text{A.30})$$

$$c_{\tilde{\chi}} = \frac{C_3}{(8a - \frac{8}{3}C_2)^{\frac{1}{2}}}, \quad (\text{A.31})$$

$$d_{\tilde{\chi}} = \frac{1}{4}(\tilde{m}_1 + \tilde{m}_2), \quad (\text{A.32})$$

and a , C_2 and C_3 are defined in [17] with the substitution $\mu \rightarrow -\mu$.

The mass mixing matrices are then given by [7, 31]:

$$Z_f = \begin{bmatrix} \cos \theta_f & -e^{-i\beta_f} \sin \theta_f \\ e^{i\beta_f} \sin \theta_f & \cos \theta_f \end{bmatrix}, \quad (\text{A.33})$$

where:

$$\tan \theta_f = \frac{c_f}{b_f}. \quad (\text{A.34})$$

When μ is chosen as real, the phase β_f is given by:

$$\tan \beta_f = \frac{-|A_f| \sin \theta_{A_f}}{\mu R_f + |A_f| \cos \theta_{A_f}}, \quad (\text{A.35})$$

where $\theta_{A_f} = \arg(A_f)$.

The charginos mixing matrices are given by [17, 7]:

$$Z^- = O_-^T, \quad Z^+ = \begin{cases} (O_+)^{-1} & \text{if } \det(M_{\tilde{\chi}}) \geq 0 \\ (\sigma_3 O_+)^{-1} & \text{if } \det(M_{\tilde{\chi}}) < 0 \end{cases}, \quad (\text{A.36})$$

where:

$$O_{\pm} = \begin{pmatrix} \cos \phi_{\pm} & \sin \phi_{\pm} \\ -\sin \phi_{\pm} & \cos \phi_{\pm} \end{pmatrix}, \quad (\text{A.37})$$

and:

$$\tan 2\phi_- = 2\sqrt{2}M_W \frac{\mu \sin \beta + \tilde{m}_2 \cos \beta}{m_2^2 - \mu^2 - 2M_W^2 \cos 2\beta}, \quad (\text{A.38})$$

$$\tan 2\phi_+ = 2\sqrt{2}M_W \frac{\mu \cos \beta + \tilde{m}_2 \sin \beta}{m_2^2 - \mu^2 + 2M_W^2 \cos 2\beta} . \quad (\text{A.39})$$

The neutralinos mixing matrix elements are given by [17]:

$$\frac{N_{i2}}{N_{i1}} = \frac{1}{\tan \theta_W} \times \frac{\tilde{m}_1 - \epsilon_i m_{\tilde{\chi}_i^0}}{\tilde{m}_2 - \epsilon_i m_{\tilde{\chi}_i^0}} , \quad (\text{A.40})$$

$$\frac{N_{i3}}{N_{i1}} = \frac{\mu[\tilde{m}_2 - \epsilon_i m_{\tilde{\chi}_i^0}][\tilde{m}_1 - \epsilon_i m_{\tilde{\chi}_i^0}] - M_Z^2 \sin \beta \cos \beta [(\tilde{m}_1 - \tilde{m}_2) \cos^2 \theta_W + \tilde{m}_2 - \epsilon_i m_{\tilde{\chi}_i^0}]}{M_Z[\tilde{m}_2 - \epsilon_i m_{\tilde{\chi}_i^0}] \sin \theta_W [\mu \cos \beta + \epsilon_i m_{\tilde{\chi}_i^0} \sin \beta]} , \quad (\text{A.41})$$

$$\frac{N_{i4}}{N_{i1}} = \frac{-\epsilon_i m_{\tilde{\chi}_i^0}[\tilde{m}_2 - \epsilon_i m_{\tilde{\chi}_i^0}][\tilde{m}_1 - \epsilon_i m_{\tilde{\chi}_i^0}] - M_Z^2 \cos^2 \beta [(\tilde{m}_1 - \tilde{m}_2) \cos^2 \theta_W + \tilde{m}_2 - \epsilon_i m_{\tilde{\chi}_i^0}]}{M_Z[\tilde{m}_2 - \epsilon_i m_{\tilde{\chi}_i^0}] \sin \theta_W [\mu \cos \beta + \epsilon_i m_{\tilde{\chi}_i^0} \sin \beta]} , \quad (\text{A.42})$$

$$N_{i1} = \left[1 + \left(\frac{N_{i2}}{N_{i1}} \right)^2 + \left(\frac{N_{i3}}{N_{i1}} \right)^2 + \left(\frac{N_{i4}}{N_{i1}} \right)^2 \right]^{-\frac{1}{2}} , \quad (\text{A.43})$$

and the relation between Z_N and N is given by Eq. A.24.

Appendix B

In this appendix we list the imaginary parts which arise from the SUSY couplings and were defined by the \mathcal{O}_k^i 's in Eqs. 22-33, Eqs. 44-51 and Eqs. 55-62 (k stands for the corresponding diagram in Fig. 2, i.e. $k = a, b, c, d, a', b', c', d', e, f, g, h$). These contain the necessary CP-odd SUSY phases needed for both the production cross-section asymmetry, A_P , and the decay PRA in the top decay, A_D .

$$\mathcal{O}_a^1 \equiv |Z_b^{1j}|^2 \text{Im} \left\{ \xi_t^i \right\} , \quad (\text{B.1})$$

$$\mathcal{O}_b^1 \equiv -\frac{1}{2} |Z_b^{1j}|^2 \text{Im} \left\{ L^- \left(|Z_t^{1i}|^2 L^{+*} + \frac{m_t}{M_W \sin \beta} Z_N^{4n*} \xi_t^i \right) \right\} , \quad (\text{B.2})$$

$$\mathcal{O}_b^2 \equiv \frac{1}{2} |Z_b^{1j}|^2 \text{Im} \left\{ L^- \left(\frac{4}{3} \tan \theta_W Z_N^{1n} \xi_t^i - \frac{m_t}{M_W \sin \beta} |Z_t^{1i}|^2 Z_N^{4n} \right) \right\} , \quad (\text{B.3})$$

$$\mathcal{O}_c^1 \equiv |Z_b^{1j}|^2 \text{Im} \left\{ Z_{1m}^{-*} L^- K^+ \right\} , \quad (\text{B.4})$$

$$\mathcal{O}_c^2 \equiv -\frac{1}{\sqrt{2}} \frac{m_t}{M_W \sin \beta} |Z_b^{1j}|^2 \text{Im} \left\{ Z_{2m}^+ L^- K^+ \right\} , \quad (\text{B.5})$$

$$\mathcal{O}_c^3 \equiv -\frac{1}{\sqrt{2}} \frac{m_t}{M_W \sin \beta} |Z_b^{1j}|^2 \text{Im} \left\{ Z_{2m}^+ L^- K^- \right\} , \quad (\text{B.6})$$

$$\mathcal{O}_c^4 \equiv |Z_b^{1j}|^2 \text{Im} \left\{ Z_{1m}^{-*} L^- K^- \right\} , \quad (\text{B.7})$$

$$\mathcal{O}_d^1 \equiv -\text{Im} \left\{ K^- M^1 \right\} , \quad (\text{B.8})$$

$$\mathcal{O}_d^2 \equiv \text{Im} \left\{ K^- M^2 \right\} , \quad (\text{B.9})$$

$$\mathcal{O}_d^3 \equiv \text{Im} \left\{ K^+ M^2 \right\} , \quad (\text{B.10})$$

$$\mathcal{O}_d^4 \equiv -\text{Im} \left\{ K^+ M^1 \right\} , \quad (\text{B.11})$$

$$\mathcal{O}_{b'}^1 \equiv -\frac{1}{2} |Z_u^{1l}|^2 |Z_d^{1o}|^2 \text{Im} \left\{ L^+ L^{-*} \right\} , \quad (\text{B.12})$$

$$\mathcal{O}_{c'}^1 \equiv |Z_d^{1o}|^2 \text{Im} \left\{ Z_{1m}^- L^{-*} K^{+*} \right\} , \quad (\text{B.13})$$

$$\mathcal{O}_{c'}^2 \equiv |Z_d^{1o}|^2 \text{Im} \left\{ Z_{1m}^- L^{-*} K^{-*} \right\} , \quad (\text{B.14})$$

$$\mathcal{O}_{d'}^1 \equiv |Z_u^{1l}|^2 \text{Im} \left\{ Z_{1m}^{+*} L^+ K^{-*} \right\} , \quad (\text{B.15})$$

$$\mathcal{O}_{d'}^2 \equiv |Z_u^{1l}|^2 \text{Im} \left\{ Z_{1m}^{+*} L^+ K^{+*} \right\} , \quad (\text{B.16})$$

$$\mathcal{O}_e^1 \equiv \frac{1}{\sqrt{2}} |Z_u^{1l}|^2 \text{Im} \left\{ Z_{1m}^{+*} L^+ M^2 \right\} , \quad (\text{B.17})$$

$$\mathcal{O}_e^2 \equiv -\frac{1}{\sqrt{2}} |Z_u^{1l}|^2 \text{Im} \left\{ Z_{1m}^{+*} L^+ M^1 \right\} , \quad (\text{B.18})$$

$$\mathcal{O}_f^1 \equiv -\frac{1}{2} \frac{m_t}{M_W \sin \beta} |Z_b^{1j}|^2 |Z_d^{1o}|^2 |L^-|^2 \text{Im} \{ Z_{1m}^- Z_{2m}^+ \} , \quad (\text{B.19})$$

$$\mathcal{O}_g^1 \equiv -\frac{1}{\sqrt{2}} |Z_d^{1o}|^2 \text{Im} \{ Z_{1m}^- L^{-*} M^1 \} , \quad (\text{B.20})$$

$$\mathcal{O}_g^2 \equiv \frac{1}{\sqrt{2}} |Z_d^{1o}|^2 \text{Im} \{ Z_{1m}^- L^{-*} M^2 \} , \quad (\text{B.21})$$

$$\mathcal{O}_h^1 \equiv \frac{1}{\sqrt{2}} |Z_u^{1l}|^2 |Z_b^{1j}|^2 \text{Im} \{ L^- L^+ Z_{1m}^{-*} Z_{1m}^{+*} \} , \quad (\text{B.22})$$

$$\mathcal{O}_h^2 \equiv -\frac{1}{2} \frac{m_t}{M_W \sin \beta} |Z_u^{1l}|^2 |Z_b^{1j}|^2 \text{Im} \{ L^- L^+ Z_{1m}^{+*} Z_{2m}^+ \} . \quad (\text{B.23})$$

In order to avoid any confusions we chose the following notation for the indexes of different squark mass eigenstates: $i, j, l, o = 1, 2$ are the indices for the two superpartners of the t, b, u, d , respectively, $m = 1, 2$ is the index for the two mass eigenstates of the charginos and $n = 1 - 4$ is the index for the four neutralinos mass eigenstates. Also L^\pm, K^+ and K^- are defined in Eqs. A.9–A.11 and:

$$\xi_t^i \equiv Z_t^{1i*} Z_t^{2i} , \quad (\text{B.24})$$

$$M^1 \equiv \frac{1}{\sqrt{2}} \frac{m_t}{M_W \sin \beta} \left(Z_{2m}^+ L^{+*} \xi_t^{i*} - \sqrt{2} Z_{1m}^+ Z_N^{4n*} \xi_t^i \right) + \frac{1}{\sqrt{2}} \left(\left(\frac{m_t}{M_W \sin \beta} \right)^2 |Z_t^{2i}|^2 Z_{2m}^+ Z_N^{4n*} - \sqrt{2} |Z_t^{1i}|^2 Z_{1m}^+ L^{+*} \right) , \quad (\text{B.25})$$

$$M^2 \equiv \frac{1}{\sqrt{2}} \frac{m_t}{M_W \sin \beta} \left(\frac{4}{3} \tan \theta_W |Z_t^{2i}|^2 Z_{2m}^+ Z_N^{1n} + \sqrt{2} |Z_t^{1i}|^2 Z_{1m}^+ Z_N^{4n} \right) - \left(\frac{1}{\sqrt{2}} \left(\frac{m_t}{M_W \sin \beta} \right)^2 Z_{2m}^+ Z_N^{4n} \xi_t^{i*} + \frac{4}{3} \tan \theta_W Z_{1m}^+ Z_N^{1n} \xi_t^i \right) . \quad (\text{B.26})$$

Appendix C

In this appendix we give the coefficients C_{pq}^k , D_{pq}^k and C_0^k , D_0^k which appear in Eqs. 22-33, Eqs. 44-51 and Eqs. 55-62 (k stands for the corresponding diagram in Fig. 2, i.e. $k = a, b, c, d, a', b', c', d', e, f, g$ and h and $p = 1, 2$, $q = 1 - 7$). These coefficients which are functions of masses and momenta are defined by the one-loop momentum integrals as follows [32]:

$$\begin{aligned} C_0; C_\mu; C_{\mu\nu}(m_1^2, m_2^2, m_3^2, p_1^2, p_2^2, p_3^2) &\equiv \\ &\equiv \int \frac{d^4k}{i\pi^2} \frac{1; k_\mu; k_\mu k_\nu}{[k^2 - m_1^2][(k + p_1)^2 - m_2^2][(k - p_3)^2 - m_3^2]} , \end{aligned} \quad (\text{B.1})$$

$$\begin{aligned} D_0; D_\mu; D_{\mu\nu}(m_1^2, m_2^2, m_3^2, m_4^2, p_1^2, p_2^2, p_3^2, p_4^2, (p_1 + p_2)^2, (p_2 + p_3)^2) &\equiv \\ &\equiv \int \frac{d^4k}{i\pi^2} \frac{1; k_\mu; k_\mu k_\nu}{[k^2 - m_1^2][(k + p_1)^2 - m_2^2][(k + p_1 + p_2)^2 - m_3^2][(k - p_4)^2 - m_4^2]} , \end{aligned} \quad (\text{B.2})$$

where $\sum_i p_i = 0$ is to be understood above.

The coefficients are then defined through the following relations [33]:

$$C_\mu = p_{1\mu} C_{11} + p_{2\mu} C_{12} , \quad (\text{B.3})$$

$$C_{\mu\nu} = p_{1\mu} p_{1\nu} C_{21} + p_{2\mu} p_{2\nu} C_{22} + \{p_1 p_2\}_{\mu\nu} C_{23} + g_{\mu\nu} C_{24} , \quad (\text{B.4})$$

$$D_\mu = p_{1\mu} D_{11} + p_{2\mu} D_{12} + p_{3\mu} D_{13} , \quad (\text{B.5})$$

$$\begin{aligned} D_{\mu\nu} = p_{1\mu} p_{1\nu} D_{21} + p_{2\mu} p_{2\nu} D_{22} + p_{3\mu} p_{3\nu} D_{23} + \{p_1 p_2\}_{\mu\nu} D_{24} + \\ + \{p_1 p_3\}_{\mu\nu} D_{25} + \{p_2 p_3\}_{\mu\nu} D_{26} + g_{\mu\nu} D_{27} , \end{aligned} \quad (\text{B.6})$$

where $\{ab\}_{\mu\nu} \equiv a_\mu b_\nu + a_\nu b_\mu$.

With the above definitions and notation, the coefficients C_0^k 's and C_{pq}^k 's for the triangle diagrams in the production amplitude which appear in Eqs. 22-33, are given by:

$$C_0^a; C_{pq}^a = \text{Im} \left\{ C_0; C_{pq}(m_G^2, m_{b_j}^2, m_{t_i}^2, m_b^2, \hat{s}, m_t^2) \right\} , \quad (\text{B.7})$$

$$C_0^b; C_{pq}^b = C_0^a; C_{pq}^a(m_G \rightarrow m_{\tilde{\chi}_n^0}) , \quad (\text{B.8})$$

$$C_0^c; C_{pq}^c = \text{Im} \left\{ C_0; C_{pq}(m_{b_j}^2, m_{\tilde{\chi}_n^0}^2, m_{\tilde{\chi}_m}^2, m_b^2, \hat{s}, m_t^2) \right\} , \quad (\text{B.9})$$

$$C_0^d; C_{pq}^d = C_0^c; C_{pq}^c(m_{\bar{b}_j} \rightarrow m_{\bar{t}_i}, m_{\tilde{\chi}_n^0} \leftrightarrow m_{\tilde{\chi}_m}) , \quad (\text{B.10})$$

$$C_0^{a'}; C_{pq}^{a'} = \text{Im} \left\{ C_0; C_{\text{pq}}(m_G^2, m_{\tilde{u}_l}^2, m_{\tilde{d}_o}^2, m_u^2, \hat{s}, m_d^2) \right\} , \quad (\text{B.11})$$

$$C_0^{b'}; C_{pq}^{b'} = C_0^{a'}; C_{pq}^{a'}(m_G \rightarrow m_{\tilde{\chi}_n^0}) , \quad (\text{B.12})$$

$$C_0^{c'}; C_{pq}^{c'} = \text{Im} \left\{ C_0; C_{\text{pq}}(m_{\tilde{d}_o}^2, m_{\tilde{\chi}_m}^2, m_{\tilde{\chi}_n^0}^2, m_u^2, \hat{s}, m_d^2) \right\} , \quad (\text{B.13})$$

$$C_0^{d'}; C_{pq}^{d'} = C_0^{c'}; C_{pq}^{c'}(m_{\tilde{d}_o} \rightarrow m_{\tilde{u}_l}, m_{\tilde{\chi}_n^0} \leftrightarrow m_{\tilde{\chi}_m}) . \quad (\text{B.14})$$

The D_0^k 's and D_{pq}^k 's, for the box diagrams in the production amplitudes which appear in Eqs. 44-51, are given by:

$$D_0^e; D_{pq}^e = \text{Im} \left\{ D_0; D_{\text{pq}}(m_{\tilde{\chi}_n^0}^2, m_{\tilde{t}_i}^2, m_{\tilde{\chi}_m}^2, m_{\tilde{u}_l}^2, m_t^2, m_b^2, m_d^2, m_u^2, \hat{s}, \hat{t}) \right\} , \quad (\text{B.15})$$

$$D_0^f; D_{pq}^f = D_0^e; D_{pq}^e(m_{\tilde{t}_i} \rightarrow m_{\bar{b}_j}, m_{\tilde{u}_l} \rightarrow m_{\tilde{d}_o}, m_{\tilde{\chi}_n^0} \leftrightarrow m_{\tilde{\chi}_m}) , \quad (\text{B.16})$$

$$D_0^g; D_{pq}^g = D_0^e; D_{pq}^e(m_{\tilde{u}_l} \rightarrow m_{\tilde{d}_o}, m_u \leftrightarrow m_d, \hat{t} \rightarrow \hat{u}) , \quad (\text{B.17})$$

$$D_0^h; D_{pq}^h = D_0^g; D_{pq}^g(m_{\tilde{t}_i} \rightarrow m_{\bar{b}_j}, m_{\tilde{d}_o} \rightarrow m_{\tilde{u}_l}, m_{\tilde{\chi}_n^0} \leftrightarrow m_{\tilde{\chi}_m}) , \quad (\text{B.18})$$

and for the top decay amplitudes, the coefficients C_0^k 's and C_{pq}^k 's which appear in Eqs. 55-62, are given by:

$$C_0^a; C_{pq}^a = \text{Im} \left\{ C_0; C_{\text{pq}}(m_{\bar{b}_j}^2, m_{\tilde{t}_i}^2, m_G^2, m_W^2, m_t^2, m_b^2) \right\} , \quad (\text{B.19})$$

$$C_0^b; C_{pq}^b = C_0^a; C_{pq}^a(m_G \rightarrow m_{\tilde{\chi}_n^0}) , \quad (\text{B.20})$$

$$C_0^c; C_{pq}^c = \text{Im} \left\{ C_0; C_{\text{pq}}(m_{\tilde{\chi}_n^0}^2, m_{\tilde{\chi}_m}^2, m_{\bar{b}_j}^2, m_W^2, m_t^2, m_b^2) \right\} , \quad (\text{B.21})$$

$$C_0^d; C_{pq}^d = C_0^c; C_{pq}^c(m_{\bar{b}_j} \rightarrow m_{\tilde{t}_i}, m_{\tilde{\chi}_n^0} \leftrightarrow m_{\tilde{\chi}_m}) . \quad (\text{B.22})$$

For the numerical evaluation of the above form factors see [32].

References

- [1] A. P. Heinson, A. S. Belyaev and E. E. Boos, hep-ph/9612424.
- [2] D. Atwood, S. Bar-Shalom, G. Eilam and A. Soni, Phys. Rev. **D54**, 5412 (1996).
- [3] Review of Particle Properties, Phys. Rev. **D50**, 1173 (1994).
- [4] For example see: T. Falk, Nucl. Phys. Proc. Suppl. **52A**, 78 (1997).
- [5] R. Garisto and J. D. Wells, Phys. Rev. **D55**, 1611 (1997).
- [6] Y. Grossman, Y. Nir and R. Rattazzi, hep-ph/9701231.
- [7] Y. Kizukuri and N. Oshimo, Phys. Rev. **D46**, 3025 (1992).
- [8] M. Aoki, A. Sugamoto and N. Oshimo, hep-ph/9706287.
- [9] B. Grzadkowski and W. Y. Keung, Phys. Lett. **B319**, 526 (1993); E. Christova and M. Fabbrichesi, Phys. Lett. **B320**, 229 (1994).
- [10] J. Ellis and R. Flores, Phys. Lett. **B377**, 83 (1996).
- [11] L. Alvarez-Gaume, J. Polchinski and M. B. Wise, Nucl. Phys. **B221**, 495 (1983).
- [12] For a review see: H. P. Nilles, Phys. Rep. **110**, 1 (1984); H. E. Haber and G. L. Kane, Phys. Rep. **117**, 75 (1985).
- [13] J. Rosiek, Phys. Rev. **D41**, 4464 (1990).
- [14] For recent reviews see: X. Tata, hep-ph/9510287; H. Baer *et al.*, hep-ph/9503479.
- [15] M. Dugan, B. Grinstein and L. Hall, Nucl. Phys. **B255**, 413 (1985).
- [16] For a recent phenomenological review of supersymmetry and reported limits obtained from LEP and Tevatron see: S. Dawson, hep-ph/9612229 and references therein.
- [17] V. Barger, M. S. Berger and P. Ohmann, Phys. Rev. **D49**, 4908 (1994).

- [18] We neglect one-loop CP-violating exchanges of supersymmetric particles in which the “resonant” (on-shell) top quark is absent, e.g., between the colliding partons and the decay products of the top. Those class of diagrams are expected to yield a much smaller CP-asymmetry than the on-shell top process. Furthermore, in the narrow width approximation the interference between those should be very small and also they can be experimentally eliminated in principle by simply demanding that the W^+b invariant mass reconstructs the top.
- [19] Vernon D. Barger and Roger J. N. Phillips, “Collider Physics”, (Addison-Wesley, New York, 1987).
- [20] We want to mention that the minus sign in front of the amplitudes of the box diagrams. This appears as a consequence of the odd number of interchanges of the anticommuting fermion spinors needed to go from the ordering of the spinors in the tree-level and one-loop triangle amplitudes to that of the box amplitudes.
- [21] S. Dimopoulos and S. Thomas, Nucl. Phys. **B465**, 23 (1996).
- [22] The function $K(r)$ in Eq. 65 is slightly different from that obtained in Ref. 5. However, we find that numerically the difference is insignificant and does not change our predictions below.
- [23] See., e.g., D. Amidei *et al.*, FERMILAB-PUB-96/082; T. Stelzer and S. Willenbrock, Phys. Lett. **B357**, 125 (95); D.O. Carlson and C.P. Yuan, hep-ph/9509208.
- [24] Note that for some values of μ and m_G , some of the lines in Figs. 4–11 end rather abruptly. This occurs due to the fact that the corresponding combination of the set of values $\{\tan\beta, \mu, m_G\}$ is forbidden experimentally, that is, either the LSP is below 20 GeV or the lighter chargino is below 65 GeV.
- [25] We want to comment here on the sharp peaks in some of the Figs. 4–11. Recall that the asymmetries discussed in this paper are proportional to absorptive cuts which are sensitive to the masses of the SUSY particles in the loops. Thus, whenever such an absorptive threshold is satisfied (i.e., two SUSY particles in the loop can go on their mass-shell) these asymmetries will exhibit a drastic change in their behavior.
- [26] Note that an asymmetry smaller than 0.25% was found by GK in Ref. 9 for the more likely choice of $m_{\tilde{t}} = 300$ GeV.

- [27] We thank M. Einhorn for suggesting to us that the existing studies of CP violation (due to SUSY) in top decays deserve a careful scrutiny.
- [28] A. P. Heinson (private communication).
- [29] M. M. El Kheishen, A. A. Shafik and A. A. Aboshousha, Phys. Rev. **D45**, 4345 (1992).
- [30] J. F. Gunion and H. E. Haber, Nucl. Phys. **B272**, 1 (1986).
- [31] We neglect generation mixing, thus shrinking Z_u and Z_d from 6×6 to 2×2 matrices.
- [32] For the FF-package that was used for numerical evaluation of loop integrals see: G.J. van Oldenborgh, Comput. Phys. Commun. **66**, 1 (1991). For the algorithms used in the FF-package see: G.J. van Oldenborgh and J.A.M. Vermaseren, Z. Phys. **C46**, 425 (1990).
- [33] G. Passarino and M. Veltman, Nucl. Phys. **B160**, 151 (1979).

Figure Captions

Fig. 1: The tree-level Feynman diagram contributing to $u\bar{d} \rightarrow t\bar{b}$.

Fig. 2: The CP-violating, SUSY induced, one-loop diagrams for the processes $u\bar{d} \rightarrow t\bar{b}$ and $t \rightarrow W^+b$.

Fig. 3: The allowed regions in the $\sin \alpha_u - \sin \alpha_d$ plane for the NEDM not to exceed a) 1.1×10^{-25} e-cm and b) 3×10^{-25} e-cm. $M_s = 400$ GeV and $m_G = 500$ GeV is used. The shaded areas indicate the allowed regions.

Fig. 4: The SUSY induced partially integrated cross-section asymmetry as a function of μ , for $M_s = 400$ GeV, $m_l = 50$ GeV and for $\sqrt{s} = 2$ TeV. With a) $\tan \beta = 1.5$ and b) $\tan \beta = 35$. See Ref. 24.

Fig. 5: The SUSY induced partially integrated cross-section asymmetry as a function of m_l , for several values of μ , $M_s = 400$ GeV, $m_G = 450$ GeV and for $\sqrt{s} = 2$ TeV. With a) $\tan \beta = 1.5$ and b) $\tan \beta = 35$.

Fig. 6: The SUSY induced partially integrated cross-section asymmetry as a function of m_G , for several values of μ , $M_s = 400$ GeV, $m_l = 50$ GeV and for $\sqrt{s} = 2$ TeV. With a) $\tan \beta = 1.5$ and b) $\tan \beta = 35$.

Fig. 7: The SUSY induced partially integrated cross-section asymmetry as a function of $\tan \beta$, for several values of μ , $M_s = 400$ GeV, $m_l = 50$ GeV and for $\sqrt{s} = 2$ TeV. With a) $m_G = 350$ GeV and b) $m_G = 350$ GeV.

Fig. 8: The SUSY induced partial rate asymmetry in the top decays as a function of μ , $M_s = 400$ GeV, $m_G = 350$ GeV and for $\sqrt{s} = 2$ TeV. With a) $\tan \beta = 1.5$ and b) $\tan \beta = 35$. See Ref. 24.

Fig. 9: The SUSY induced partial rate asymmetry in the top decays as a function of m_l , for several values of μ , $M_s = 400$ GeV and for $\sqrt{s} = 2$ TeV. With a) $\tan \beta = 1.5$ and $\mu = -160$ GeV, and b) $\tan \beta = 35$ and $\mu = 230$ GeV.

Fig. 10: The SUSY induced partial rate asymmetry in the top decays as a function of m_G , for several values of μ , $M_s = 400$ GeV, $m_l = 50$ GeV and for $\sqrt{s} = 2$ TeV. With a) $\tan \beta = 1.5$ and b) $\tan \beta = 35$.

Fig. 11: The SUSY induced partial rate asymmetry in the top decays as a function of $\tan\beta$, for several values of μ , $M_s = 400$ GeV, $m_t = 50$ GeV and for $\sqrt{s} = 2$ TeV. With a) $m_G = 350$ GeV and b) $m_G = 350$ GeV.

Table 1: The charginos and neutralinos masses for different values of $\{\tan\beta, \mu, m_G\}$. The entries in the table are rounded to the nearest integer.

$\tan\beta$ ↓	μ (GeV) ↓	charginos and neutralinos masses						m_G ← (GeV) ↓	
		$m_{\tilde{\chi}_1}$	$m_{\tilde{\chi}_2}$	$m_{\tilde{\chi}_1^0}$	$m_{\tilde{\chi}_2^0}$	$m_{\tilde{\chi}_3^0}$	$m_{\tilde{\chi}_4^0}$		
1.5	-70	138	94	56	68	111	138	350	
		160	94	65	75	107	161	450	
		185	92	67	88	104	186	550	
	-90	140	107	56	85	128	137	350	
		160	110	70	88	124	160	450	
		184	110	81	92	122	184	550	
	-130	161	118	56	112	162	145	350	
		167	136	70	122	160	161	450	
		185	143	84	126	158	183	550	
	140	202	40	16	67	142	209	350	
		214	56	29	86	141	220	450	
		229	70	41	103	141	234	550	
	240	276	65	35	75	241	282	350	
		282	89	49	98	241	287	450	
		288	110	63	120	241	294	550	
	35	-110	176	65	41	70	132	172	350
			189	77	50	86	130	187	450
			206	86	59	100	128	205	550
-170		212	82	47	83	187	208	350	
		219	102	60	103	185	216	450	
		229	118	73	121	184	227	550	
-190		228	85	48	86	206	223	350	
		233	107	61	107	204	229	450	
		241	125	74	127	203	238	550	
110		177	60	37	69	130	175	350	
		191	72	47	85	128	189	450	
		208	82	56	100	126	207	550	
170		214	78	45	80	185	211	350	
		221	97	58	100	184	219	450	
		231	114	70	119	183	230	550	

Fig.1

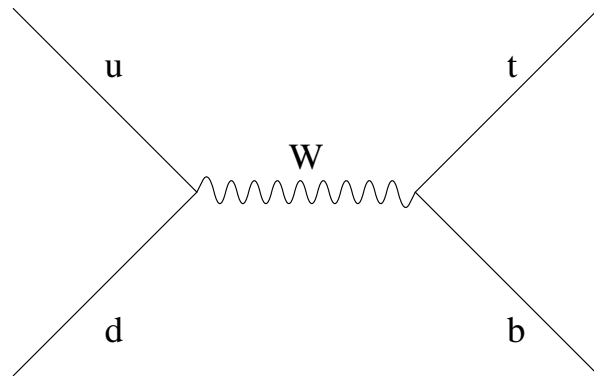


Fig.2

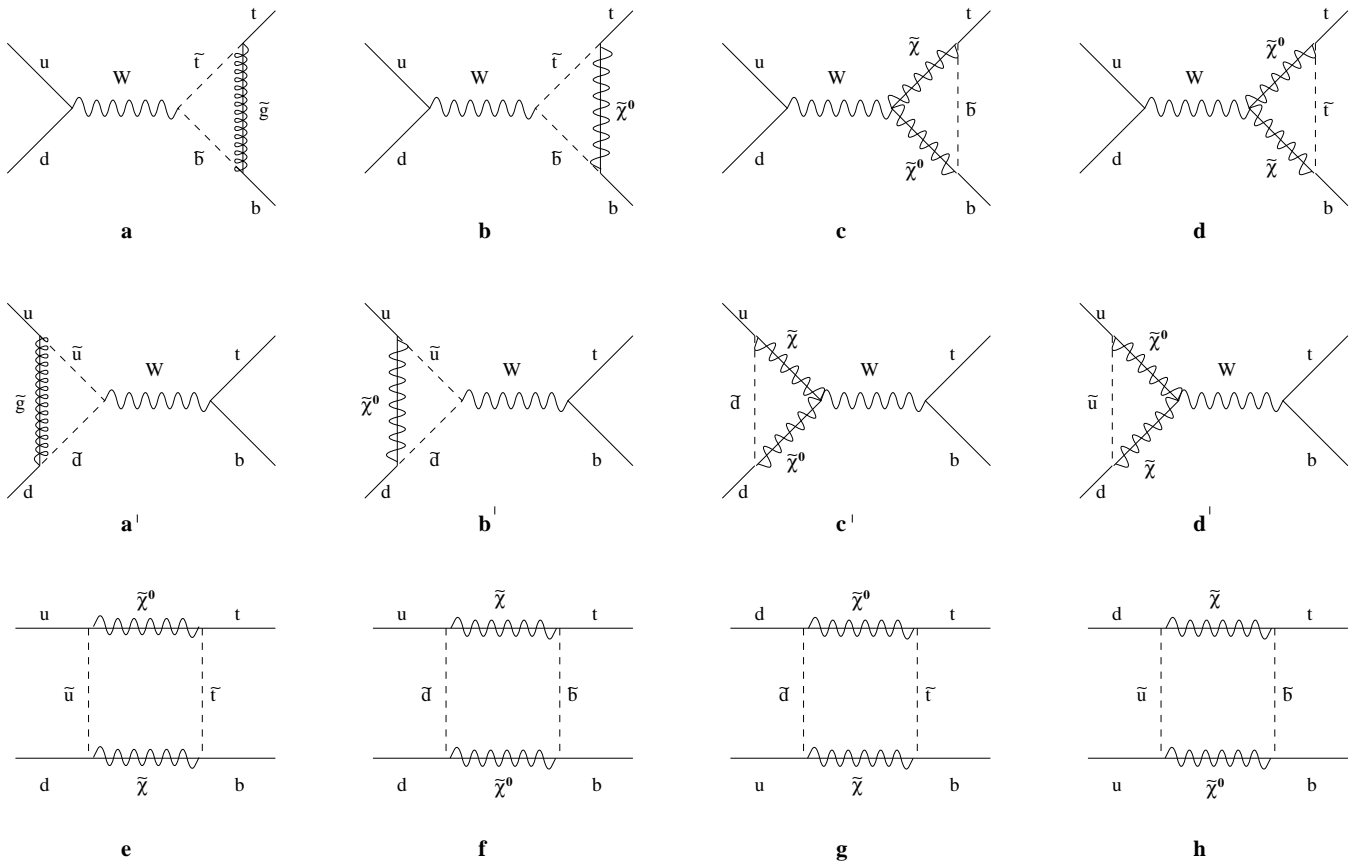


Fig.3

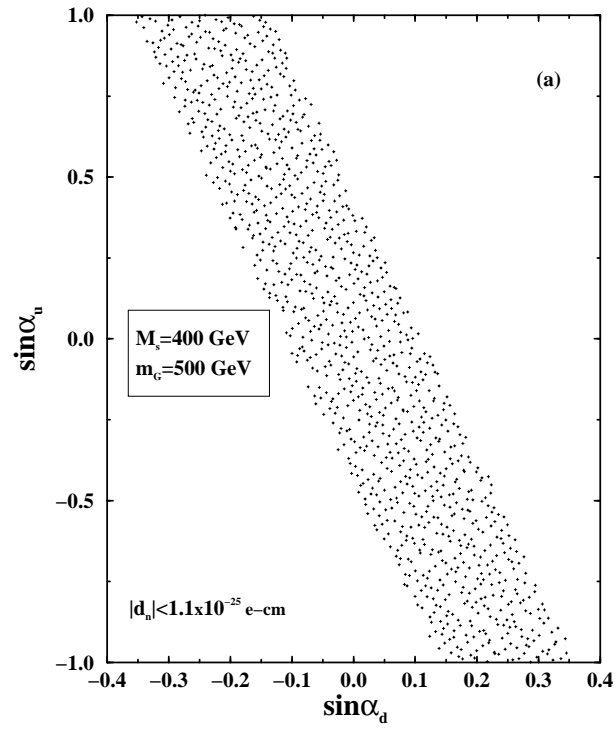


Fig.3

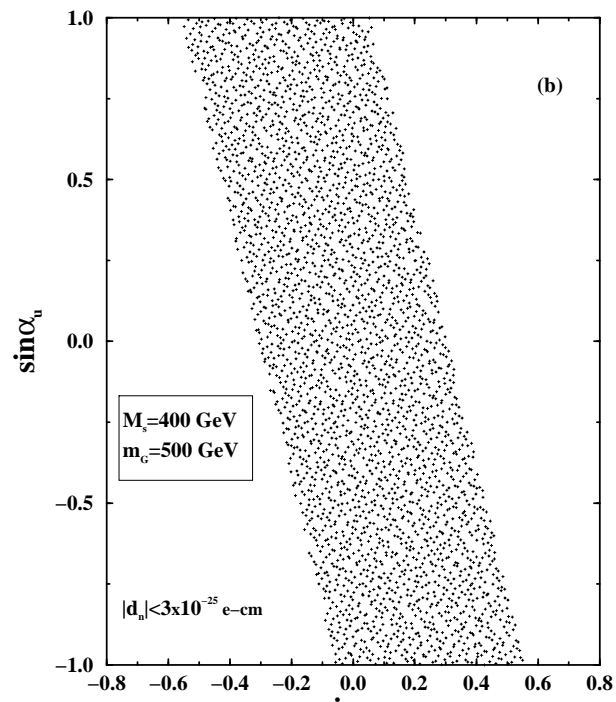


Fig.4

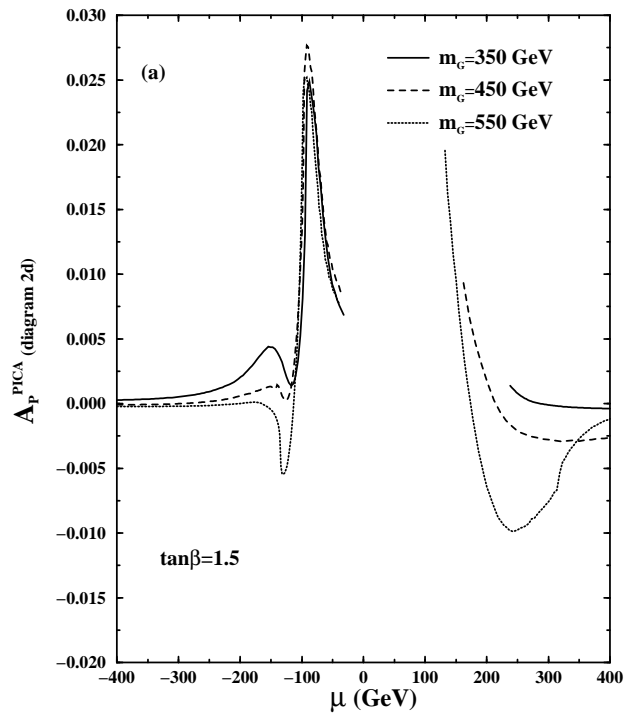


Fig.4

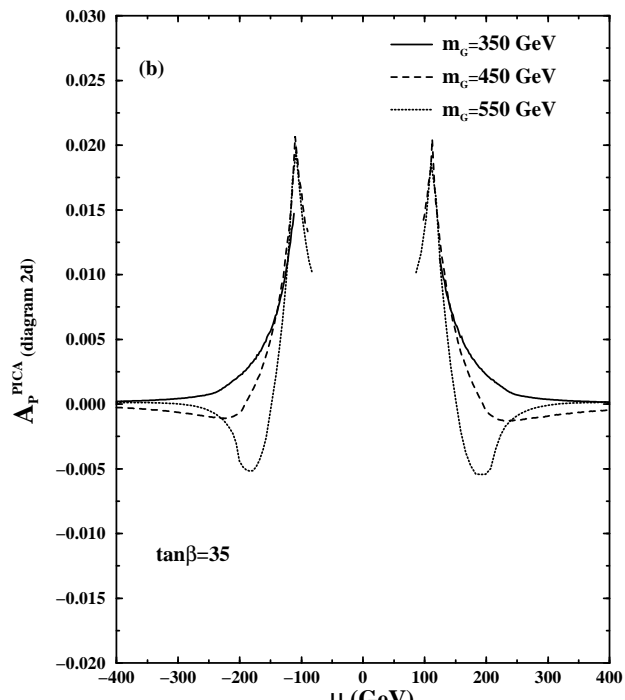


Fig.5

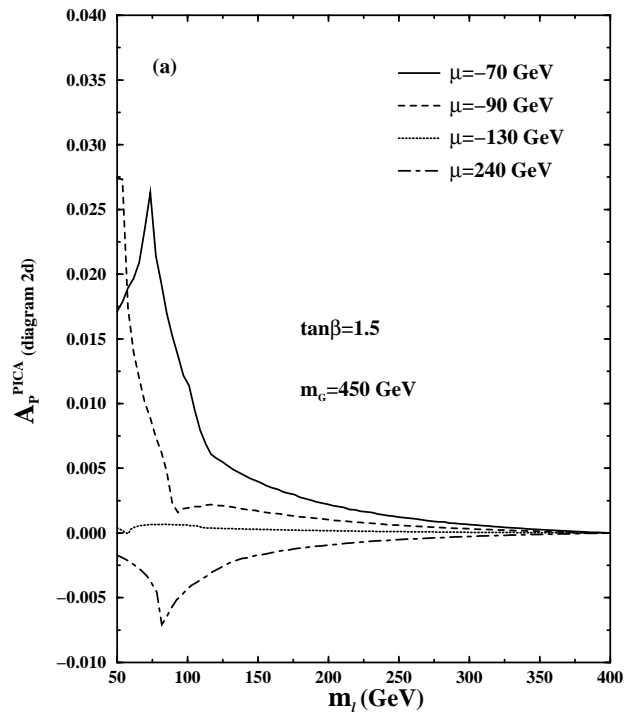


Fig.5

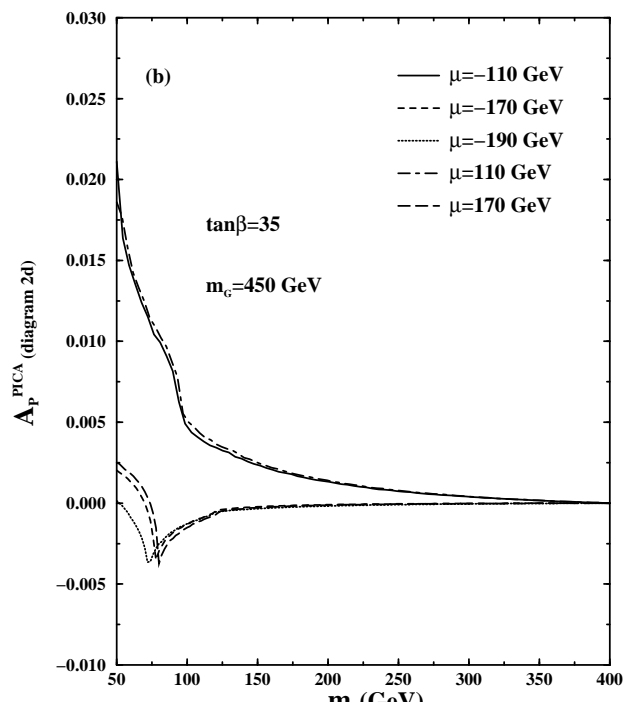


Fig.6

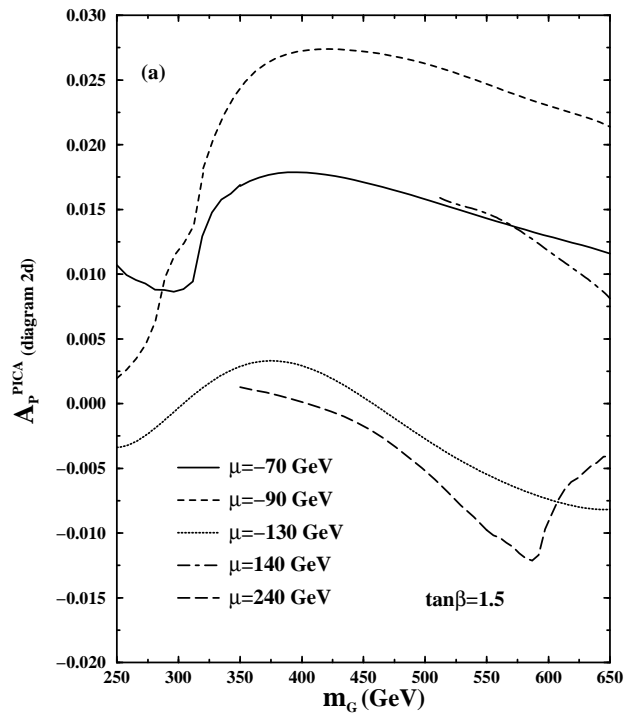


Fig.6

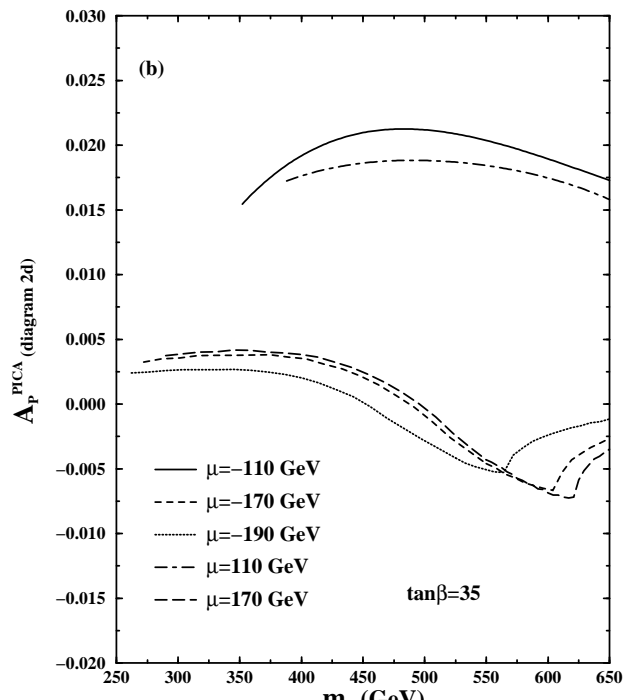


Fig.7

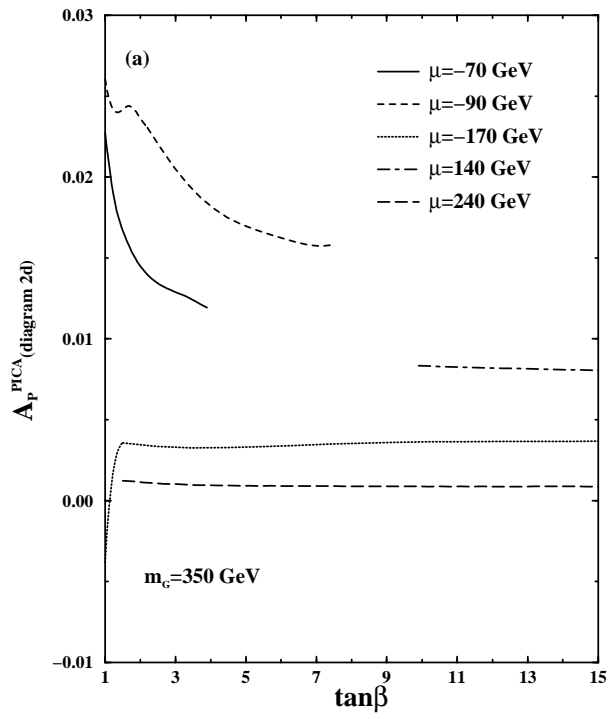


Fig.7

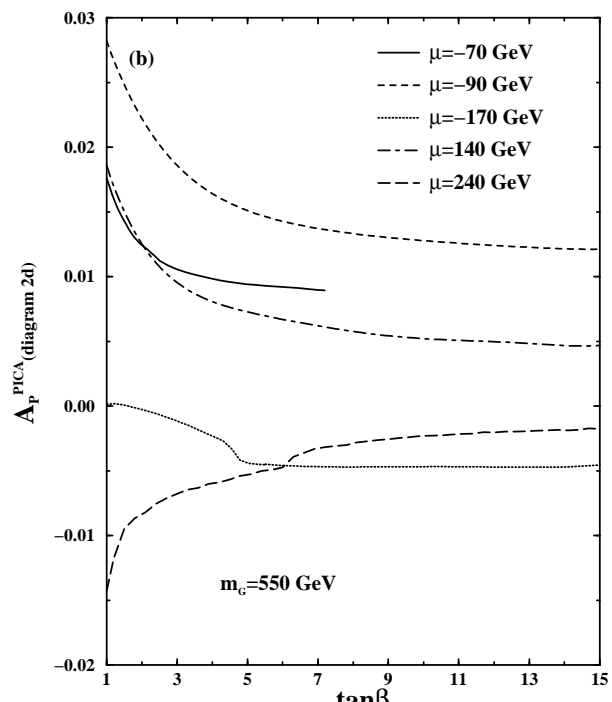


Fig.8

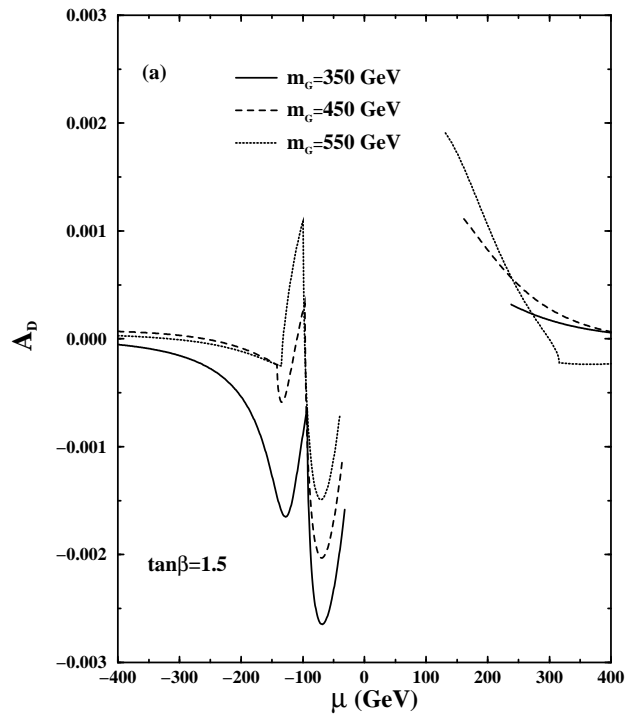


Fig.8

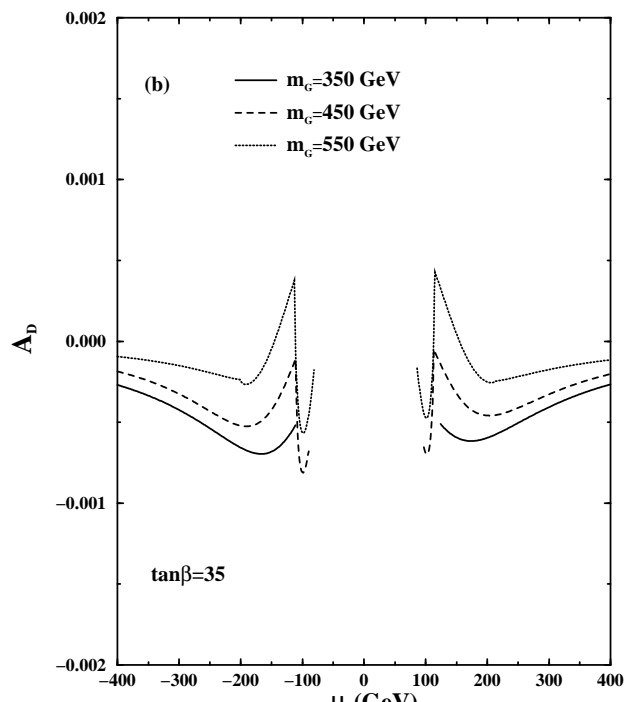


Fig.9

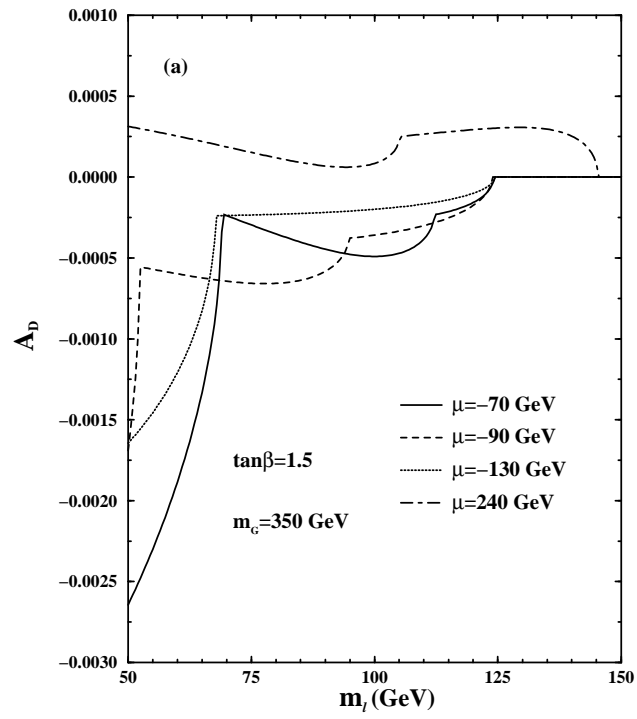


Fig.9

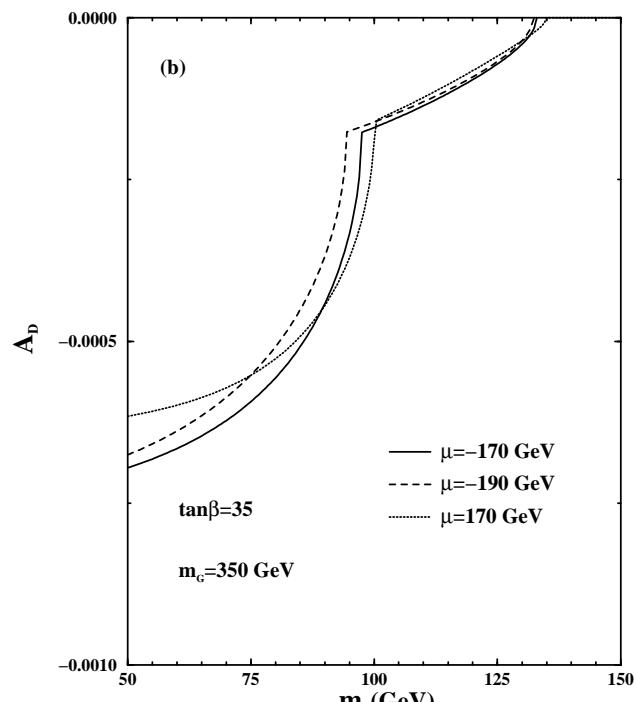


Fig.10

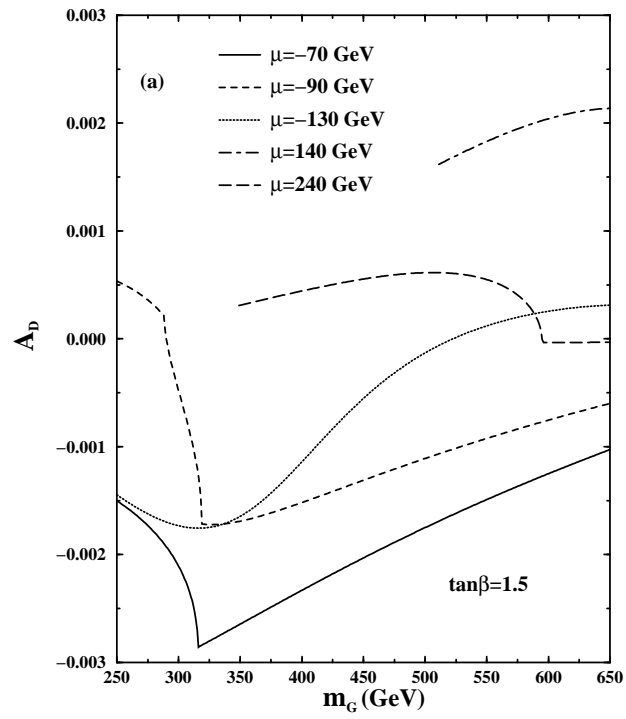


Fig.10

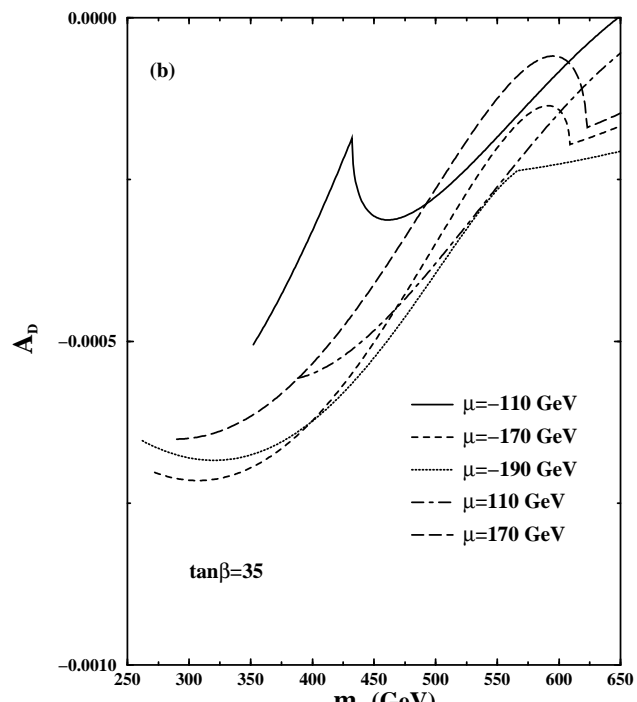


Fig.11

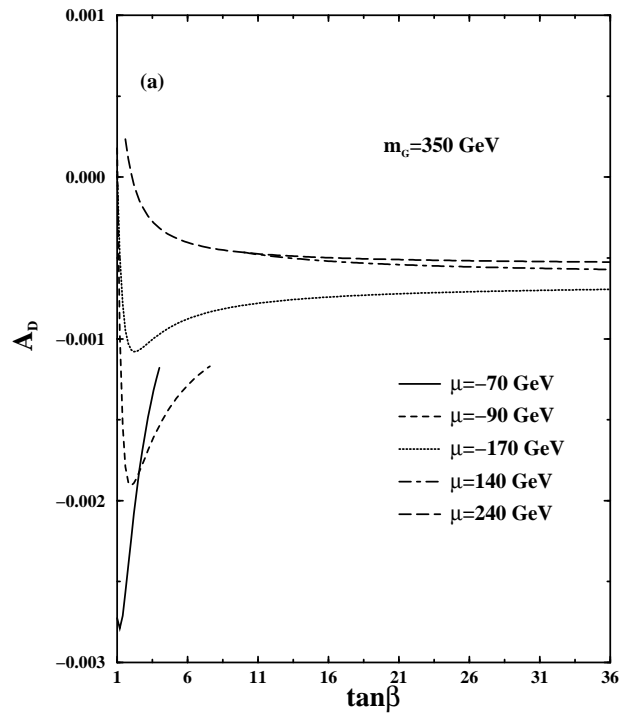


Fig.11

